

## ABSTRACT

STRATTON, BLAKE EVAN. Formation of Secondary Inorganic PM<sub>2.5</sub> as Impacted by Ammonia Concentrations near An Animal Feeding Operation. (Under the direction of Dr. Lingjuan Wang-Li).

The impact of ammonia (NH<sub>3</sub>) emissions from animal agriculture on the secondary formation of inorganic fine particulate matter (i.e., iPM<sub>2.5</sub>) has become of great public concern. The formation of iPM<sub>2.5</sub> from NH<sub>3</sub> is known as the gas-particle partitioning of gaseous NH<sub>3</sub> and aerosol ammonium (NH<sub>4</sub><sup>+</sup>), which is assumed to be in a thermodynamic equilibrium. This research aimed to gain an in-depth understanding of the impact of ambient NH<sub>3</sub> on secondary iPM<sub>2.5</sub> by analyzing the PM<sub>2.5</sub> mass closure, atmospheric chemical conditions, and the gas particle partitioning of NH<sub>3</sub>-NH<sub>4</sub><sup>+</sup> in the near field of a poultry production unit in North Carolina. Samples of precursor gases (i.e., NH<sub>3</sub>, SO<sub>2</sub>, NO<sub>2</sub>) to iPM<sub>2.5</sub> and PM<sub>2.5</sub> were taken on this poultry production unit at four sampling stations in four wind directions through summer, autumn and winter seasons to determine gas concentrations and PM<sub>2.5</sub> chemical compositions. It was discovered that this rural site contained low ambient concentrations of iPM<sub>2.5</sub> precursor gases, and PM<sub>2.5</sub> composition was dominated by organic carbon (OC) (80% to 94%) while iPM<sub>2.5</sub> fraction was insignificant (0% to 2%). Low availability of H<sub>2</sub>SO<sub>4</sub> and HNO<sub>3</sub> gases (from SO<sub>2</sub> and NO<sub>2</sub> conversions) limited NH<sub>3</sub> neutralization potential and iPM<sub>2.5</sub> formation; moreover, high OC fraction may inhibit NH<sub>4</sub><sup>+</sup> formation. With the field measurements of ambient temperature, humidity, precursor gases and PM<sub>2.5</sub> chemical speciation data, the ISORROPIA-II thermodynamic equilibrium model was used to conduct sensitivity analysis found that iPM<sub>2.5</sub> was the most sensitive to increasing total HNO<sub>3</sub> (gas + aerosol) at low temperatures. The formation potential of iPM<sub>2.5</sub> at this rural site was at its highest during the wintertime when SO<sub>2</sub> was extremely low.

© Copyright 2023 by Blake Stratton  
All Rights Reserved

Formation of Secondary Inorganic PM<sub>2.5</sub> as Impacted by Ammonia Concentrations near An  
Animal Feeding Operation.

by  
Blake Evan Stratton

A thesis submitted to the Graduate Faculty of  
North Carolina State University  
in partial fulfillment of the  
requirements for the degree of  
Master of Science

Biological and Agricultural Engineering

Raleigh, North Carolina  
2023

APPROVED BY:

---

Dr. Lingjuan Wang-Li  
Committee Chair

---

Dr. Sanjay Shah

---

Dr. Wei Shi

---

Dr. John Classen

---

Dr. Kenneth Anderson

## **BIOGRAPHY**

Blake Stratton was born and raised in Montgomery, Alabama. He attended Auburn University in Auburn, AL where he earned his bachelor's degree in Biosystems Engineering in spring 2021. He continued on into graduate school in fall 2021 at North Carolina State University to pursue a master's degree in Biological and Agricultural Engineering under the guidance of Dr. Lingjuan Wang-Li. After concluding his master's thesis, he will be starting a position as an environmental engineer for the Alabama Department of Environmental Management.

## ACKNOWLEDGEMENTS

This project was funded by National Science Foundation under NSF-CBET Award No. 1804720.

I want to thank Dr. Lingjuan Wang-Li for giving me the opportunity to join your research team as well as being a great mentor throughout my research. Thank you to my committee members, Dr. Sanjay Shah, Dr. Kenneth Anderson, Dr. Wei Shi, and Dr. John Classen for your support and expertise on this project.

I want to also thank Tracy Dombek and her team at RTI International for collaborating with us and helped analyze PM<sub>2.5</sub> mass, elements, ions, and the denuders. Thank you to the RTI team: Sophie Brenner, Katarina Lindskog, Nicole Manalis, Jason McNeill, Andrea McWilliams, and Frank Weber, for the contributions you all made to this project.

This study was possible thanks to the contributions from the following people: Lisa Wilson and all the staff members at the NC Department of Agriculture Piedmont Research Station Poultry Unit for allowing us to conduct the sampling as well as providing help when needed; Justin Macialek and Jay Campbell for helping with moving the heavy samplers; Mr. Phil Harris for helping with repairing one of the samplers; Dr. Bin Cheng, Dr. Suraiya Akter, and Sam Cherotich for the countless hours sacrificed to help me with this project; Dr. Andrew Grieshop and his research team for allowing me to use his instrumentation for PM<sub>2.5</sub> carbon analysis Last but not least, thank you to my family and friends for all of your support.

## TABLE OF CONTENTS

LIST OF TABLES .....	v
LIST OF FIGURES.....	vi
CHAPTER 1: Introduction.....	1
1.1 Background .....	1
1.2 Literature Review .....	3
1.2.1 Ammonia from Livestock and Poultry .....	3
1.2.2 Fate, Transportation, and Transformation of Atmospheric NH <sub>3</sub> .....	4
1.2.3 Atmospheric Chemical Conditions and iPM <sub>2.5</sub> formation potential .....	8
1.2.4 Thermodynamic Equilibrium Modeling.....	10
1.3 Research Gaps and Hypothesis.....	12
1.3.1 Research Gaps .....	12
1.3.2 Research hypothesis .....	13
1.4 Research objectives .....	13
CHAPTER 2: Methodology .....	14
2.1. Research Site .....	14
2.1.1 The Poultry Production Unit .....	14
2.1.2 Ambient Air Monitoring and Sampling Stations.....	15
2.2. PM <sub>2.5</sub> Chemical Speciation Sampling and Precursor Gases Sampling.....	16
2.2.1 PM <sub>2.5</sub> Chemical Speciation Sampling Method .....	16
2.2.2 Precursor Gases Sampling Methods.....	18
2.2.3 Sampling Preparation .....	20
2.2.4 Sampling in the Field .....	22
2.2.5 PM <sub>2.5</sub> and Precursor Gases Sampling Schedule .....	23
2.2.6 Post Sampling .....	24
2.3. Meteorological Data Collection .....	26
2.4. PM <sub>2.5</sub> Chemical Speciation and Passive Gas Sample Analyses .....	27
2.4.1 PM <sub>2.5</sub> Chemical Speciation Analyses .....	27
2.4.1 Precursor Gas Sample Analyses.....	29
2.5. PM <sub>2.5</sub> Chemical Species and Precursor Gas Concentration Determinations .....	29
2.5.1 Concentrations of PM <sub>2.5</sub> Chemical Species .....	29
2.5.2 NH <sub>3</sub> Concentration by Using Denuder.....	31

2.5.3 NH <sub>3</sub> , NO <sub>2</sub> , SO <sub>2</sub> Concentrations by Using Passive Samplers .....	31
2.5.4 NO <sub>2</sub> Conversion .....	32
2.6 Atmospheric Chemical Condition Analysis .....	33
2.7 PM <sub>2.5</sub> Mass Closure Analysis.....	34
2.8 ISOROPPIA-II Modeling.....	34
2.9 Statistical Analysis .....	34
CHAPTER 3: Results and Discussion.....	35
3.1 Comparison of passive samplers and denuders for NH <sub>3</sub> measurements .....	35
3.2 Atmospheric Chemical Conditions.....	37
3.2.1 Spatial and Temporal Variations of GR & AdjGR as Impacted by Wind Direction .....	38
3.2.2 Spatial and temporal variations of PNR as Impacted by Wind Direction .....	40
3.2.3 Spatial and temporal variations of NH <sub>3</sub> /NH <sub>x</sub> as Impacted by Wind Direction.....	41
3.2.4 Spatial and temporal variations of TA/TS as Impacted by Wind Direction .....	42
3.2.5 Spatial and temporal variations of AN/PM <sub>2.5</sub> as Impacted by Wind Direction .....	43
3.3 PM <sub>2.5</sub> Mass Closure .....	45
3.4 ISOROPPIA-II Modeling.....	51
3.4.1 Modeling with Passive Sampler HNO <sub>3</sub> .....	51
3.4.2 Modeling with Chemical Speciation Data.....	54
3.4.3 Response of Secondary iPM <sub>2.5</sub> to Total NH <sub>3</sub> .....	57
3.4.4 Response of Secondary iPM <sub>2.5</sub> to Total NO <sub>3</sub> .....	59
CHAPTER 4: Conclusions and Future Work.....	62
References .....	64

## LIST OF TABLES

Table 2.1.	Sampling event summary .....	24
Table 2.2.	Meteorological data at the research site.....	27
Table 2.3.	PM <sub>2.5</sub> chemical speciation species and methods .....	27
Table 2.4.	NO <sub>2</sub> molar ratios .....	33
Table 3.1.	NH <sub>3</sub> concentrations measure through sampling by Denuders .....	36
Table 3.2.	NO <sub>2</sub> and SO <sub>2</sub> concentrations measured by Ogawa passive sampler.....	37
Table 3.3.	Mean ±SD of the chemical condition metrics separated by season and location.....	38
Table 3.4.	Mean ± SD for PM <sub>2.5</sub> and its Components in µg/m <sup>3</sup> .....	46
Table 3.5.	ISORROPPIA-II sensitivity analysis inputs.....	57

## LIST OF FIGURES

Figure 2.1.	Spatial distribution of poultry & swine farms in NC (Dietrich, 2019) and the research site location.....	14
Figure 2.2.	Research site layout and the ambient air monitoring and sampling stations .....	15
Figure 2.3.	Partisol speciation sampler (left) and filter cartridges (right).....	17
Figure 2.4.	Partisol PM <sub>2.5</sub> speciation sampler in the field (left) and its flow schematic (right)	18
Figure 2.5.	Anatomy of Ogawa passive sampler (Ogawa USA).....	19
Figure 2.6.	Application of 2% citric acid solution to coat honeycomb denuders .....	20
Figure 2.7.	Storage of Quartz (left), Nylon (middle), and Teflon (right) filters for transporting to the field .....	21
Figure 2.8.	Assembling passive samplers (left) and Ogawa airtight storage container (right).	21
Figure 2.9.	Installing filters to the cartridges in the field mobile lab.....	22
Figure 2.10.	Installing filters to the cartridges in the field mobile lab .....	23
Figure 2.11.	Storage of filters and denuders for transportation (left) and denuder samples after extraction in vials (right) .....	25
Figure 2.12.	Boxplots NH <sub>3</sub> concentrations measured by of Ogawa passive sampler and honeycomb denuder .....	35
Figure 3.1.	The AdjGR over changes of wind direction separated by sampling station and season .....	39
Figure 3.2.	The PNR over changes of wind direction separated by sampling station and season.....	41
Figure 3.3.	The NH <sub>3</sub> /NH <sub>x</sub> over changes of wind direction separated by sampling station and season.....	42
Figure 3.4.	The TA/TS over changes of wind direction separated by sampling station and season.....	43
Figure 3.5.	The AN/PM <sub>2.5</sub> over changes of wind direction separated by sampling station and season.....	45
Figure 3.6.	Summer PM <sub>2.5</sub> chemical speciation mass fractions.....	48
Figure 3.7.	Autumn PM <sub>2.5</sub> chemical speciation mass fractions .....	49

Figure 3.8. Winter PM <sub>2.5</sub> chemical speciation mass fractions .....	51
Figure 3.9. Comparison of ISORROPIA-II model results with passive sampler HNO <sub>3</sub> .....	53
Figure 3.10. Comparison of ISORROPIA-II model results with passive sampler HNO <sub>3</sub> continued .....	54
Figure 3.11. Comparison of ISORROPIA-II model results with speciation data measurements	55
Figure 3.12. ISORROPIA-II predicted aerosol Cl vs. measured total Cl .....	56
Figure 3.13. ISORROPIA-II predicted SO <sub>4</sub> <sup>-2</sup> vs. measured SO <sub>4</sub> <sup>-2</sup> under stable state conditions .....	56
Figure 3.14. Responses of iPM <sub>2.5</sub> components to total NH <sub>3</sub> under five different T and RH conditions .....	58
Figure 3.15. Responses of iPM <sub>2.5</sub> components to total NO <sub>3</sub> <sup>-</sup> under five different T and RH conditions .....	60

# CHAPTER 1: INTRODUCTION

## 1.1 BACKGROUND

One of the most important nutrients for all of life is nitrogen (N) since it is a key element for balancing ecosystems and plant growth. The most readily available forms of N for agriculture are nitrate ( $\text{NO}_3^-$ ) and ammonium ( $\text{NH}_4^+$ ) which derives from atmospheric nitrogen gas ( $\text{N}_2$ ) (Shaver et. al, 2014). A common practice is to chemically synthesize atmospheric  $\text{N}_2$  to yield ammonia ( $\text{NH}_3$ ) so that it can be directly used as a fertilizer; however, use of  $\text{NH}_3$  fertilizer can result in volatilization (Shaver et. al, 2014). Volatilization is the conversion of a liquid chemical into a vapor, which is then emitted into the atmosphere. In the United States (US), the largest source of  $\text{NH}_3$  emissions is agriculture, with sources including livestock production and fertilizer application (Behera et. al, 2013). Ma et. al, (2020) reported that 1.1 million tons of N loss per year are from synthetic fertilizers in the US, while Van Damme et al., (2021) reported that over 80% of total  $\text{NH}_3$  emissions are a result of volatilization from livestock manure and synthetic fertilizers. Emitted  $\text{NH}_3$  can enter ecosystems through wet or dry deposition and cause adverse environmental effects such as soil acidification which leads to biodiversity reduction in plants (Guthrie et al., 2018). Acidification can also make forests more vulnerable to other stress factors such as frost, drought, and pests (Bouwman et al., 2002). Deposition of  $\text{NH}_3$  can also occur on surface water bodies which increases N input and shifts plant species composition towards nitrophilic species (Bobbink et al., 1998). Long term exposure to  $\text{NH}_3$  can result in skin, nose, eye, and throat irritation (Wing and Wolf, 2000). The most important characteristic of  $\text{NH}_3$  is its role as a precursor gas to secondary inorganic fine particulate matter ( $\text{iPM}_{2.5}$ ) formation. In general, particulate matter (PM) are small particles that can vary in size and are classified as either fine ( $\text{PM}_{2.5}$ ) or coarse ( $\text{PM}_{2.5-10}$ ) PM, it may also be classified as primary or secondary.

Primary PM is directly emitted into the atmosphere from an emission source, whereas secondary PM is formed through atmospheric chemical reactions.

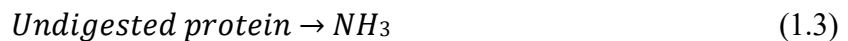
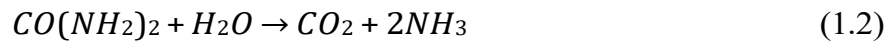
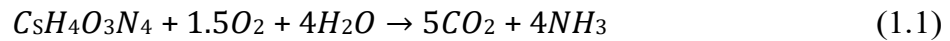
By definition, PM<sub>2.5</sub> are solid/liquid particles with an aerodynamic equivalent diameter (AED) of less than or equal to 2.5 μm. These particles include NH<sub>4</sub><sup>+</sup>, sodium (Na<sup>+</sup>), elemental carbon (EC), organic carbon (OC), chloride (Cl<sup>-</sup>), sulfate (SO<sub>4</sub><sup>-2</sup>), bisulfate (HSO<sub>4</sub><sup>-2</sup>), NO<sub>3</sub><sup>-</sup>, elements, and crustal species such as calcium (Ca<sup>+2</sup>), potassium (K<sup>+</sup>), and magnesium (Mg<sup>+2</sup>). These particles are small enough to penetrate the thoracic region of the human respiratory system, which can lead to the development of lung disease and heart disease (World Health Organization, 2013). Exposure to PM<sub>2.5</sub> can cause health effects such as respiratory and cardiovascular morbidity, and mortality from cardiovascular diseases, respiratory diseases, and lung cancer (World Health Organization, 2013). In 2010, there was an estimated 3.15 million global PM<sub>2.5</sub> related mortalities where the main causes were cerebrovascular disease (1.31 million), ischaemic heart disease (1.08 million) and secondary causes are chronic obstructive pulmonary disease (374,000), acute lower respiratory illness (230,000), and lung cancer (161,000) (Lelieveld et al., 2015). A study by Malley et al., (2021) reports that 537,000 global premature deaths were found to be associated with PM<sub>2.5</sub> as a result of agriculture emissions. Ambient PM<sub>2.5</sub> particles also can absorb or deflect light rays causing visibility reduction (haze) which is an indicator of poor air quality.

As increasingly stringent local, state, and federal air pollution regulations are likely to occur, NH<sub>3</sub> as a precursor to a criteria air pollutant, PM<sub>2.5</sub>, has become of great concern (Shaver et. al, 2014). In order for a science-based regulation to occur, additional understanding of the effects of agricultural NH<sub>3</sub> emissions on the secondary formation of iPM<sub>2.5</sub> will need to be further Investigated.

## 1.2 LITERATURE REVIEW

### 1.2.1 Ammonia from Livestock and Poultry

Agriculture contributes the majority of global NH<sub>3</sub> emissions. Van Damme et al., (2021) reported that over 80% of global NH<sub>3</sub> emissions are a result of volatilization from livestock manure (mixture of feces and urine) and synthetic fertilizers. The main sources of NH<sub>3</sub> emissions from agriculture are livestock and animal production, manure storage and handling, livestock housing, manure application, and synthetic fertilizer application (Behera et al., 2013). The N in excreted manure exists in the form of uric acid (C<sub>5</sub>H<sub>4</sub>N<sub>4</sub>O<sub>3</sub>), urea (CO(NH<sub>2</sub>)<sub>2</sub>), or undigested proteins. This N is broken down and released in the form of NH<sub>4</sub><sup>+</sup> under acidic conditions or as NH<sub>3</sub> gas at higher pH levels. The three main microbial reactions are shown in Equations 1.1- 1.3:



The volatilization of NH<sub>3</sub> can be affected by many factors such as pH, temperature, moisture content, and wind speed. The degradation of uric acid is influenced by changes in temperature or pH since they affect microbial activity. Elliot and Collins (1982) found that NH<sub>3</sub> volatilization in poultry production is affected in the order: litter pH >> temperature > moisture content. In an air emission from land application study, Sommer et al., (1991) reported that NH<sub>3</sub> loss increased linearly with wind speed and increased exponentially with temperature. NH<sub>3</sub> volatilization potential nearly doubles with every 5 °C increase in temperature. Meanwhile, NH<sub>3</sub> emissions are controlled by water availability, which allows NH<sub>3</sub> to dissolve, be taken up by organisms, and be released through decomposition (Sutton et al., 2013). Precipitation and temperature are

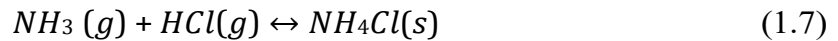
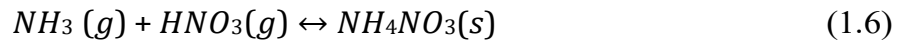
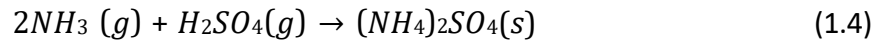
significant drivers for emissions when manure is applied on land where the emission fraction is up to 5 times larger in semi-dry tropics than in cold, wet climates (Jiang et al., 2021).

### ***1.2.2 Fate, Transportation, and Transformation of Atmospheric NH<sub>3</sub>***

Volatilized NH<sub>3</sub> has a short atmospheric residence time around 0.8 to 4 days and a high deposition velocity of up to 14 cm/s (Sutton, Fowler, & Moncrieff, 1993; Phillips et al., 2004). This means that NH<sub>3</sub> is expected to be found a short distance from its source after emission. The short residence time can be attributed to NH<sub>3</sub> adsorbing to almost all surfaces (Shaver et al., 2014) and will primarily deposit on wet surfaces and vegetation (Walker et al., 2000). NH<sub>3</sub> deposition occurs as wet or dry deposition. Dry deposition is the free fall of gas-phase NH<sub>3</sub> or particle-phase NH<sub>4</sub><sup>+</sup> to Earth from the atmosphere while wet deposition can occur in one of two different ways. Ambient NH<sub>3</sub> close to the emission source can be scavenged out inefficiently by raindrops and snow (Asman, 1994). The gaseous NH<sub>3</sub> can also mix into clouds, where NH<sub>3</sub> is transferred into cloud droplets and through microphysical processes, they will be deposited from the atmosphere as rain or snow (Asman et al., 1998). Wet and dry deposition rates and quantities depend on factors including meteorological conditions, surface conditions, and the physical and chemical properties of the gases, particles, and surfaces in question (EPA, 2017). Deposition of gaseous NH<sub>3</sub> onto vegetation can occur through leaf cuticle or plant uptake. The deposition on leaf surfaces is closely related to the presence of water on the cuticle (Sutton, Fowler, & Moncrieff, 1993). Van Hove et al., (1988) found that the adsorbed quantities of NH<sub>3</sub> on leaf cuticles increased strongly with air humidity, indicating that water on the leaf surface plays a major role in the interaction. Duyzer et al., (1994) found that NH<sub>3</sub> is highly attracted to leaf cuticles with or without the presence of water on leaves so cuticle uptake can still occur on dry leaves. Deposition of NH<sub>3</sub> can also occur on soils and can lead to acidification due to its

subsequent nitrification. Acidifying inputs, such as  $\text{NH}_3$  and  $\text{NH}_4^+$ , deposited on soils can decrease soil pH, which can hinder nitrification. Lower pH values will break down clay minerals and hydrous oxides, which leads to the accumulation of toxic aluminum ( $\text{Al}^{+3}$ ) and other metals in the soil. As a result of these changes, acid-resistant plant species will gradually become dominant, and several species typical of intermediate and higher pHs will disappear (Bobbink and Hicks, 2014)..

The major pathway to the transformation of ambient  $\text{NH}_3$  is to react with atmospheric acidic gases to form secondary  $\text{iPM}_{2.5}$ . The formation of secondary  $\text{iPM}_{2.5}$  will occur when gaseous  $\text{NH}_3$  reacts with ambient acidic gases such as sulfuric acid ( $\text{H}_2\text{SO}_4$ ), hydrochloric acid ( $\text{HCl}$ ), or nitric acid ( $\text{HNO}_3$ ) to form ammonium sulfate ( $(\text{NH}_4)_2\text{SO}_4$ ), ammonium chloride ( $\text{NH}_4\text{Cl}$ ), or ammonium nitrate  $\text{NH}_4\text{NO}_3$ , respectively. Since  $\text{NH}_3$  is a weak base and highly reactive, it will tend to neutralize acidic species in the atmosphere in a process called the gas-particle partitioning of  $\text{NH}_3\text{-NH}_4^+$ ; therefore, this reaction is highly driven by the availability of atmospheric  $\text{NH}_3$  (Bauer et al., 2016) and acidic gases. The gas-particle partitioning of  $\text{NH}_3\text{-NH}_4^+$  is shown in Equations 1.4 -1.7.



Limited availability of  $\text{NH}_3$  may also result in partial neutralizing of  $\text{H}_2\text{SO}_4$  to form  $\text{HSO}_4^-$  or  $\text{SO}_4^{2-}$  salts (Cheng et al., 2021). Due to the low vapor pressure of  $\text{H}_2\text{SO}_4$ , it is hardly ever found in the gas phase and typically reacts with  $\text{NH}_3$  to become  $\text{SO}_4^{2-}$  (Koziel et al., 2006).

HNO<sub>3</sub> is more volatile than H<sub>2</sub>SO<sub>4</sub>, so NO<sub>3</sub><sup>-</sup> is believed to be in lower concentrations than SO<sub>4</sub><sup>-2</sup> (Pacyna et al., 1996). The equilibrium of NH<sub>4</sub>Cl and NH<sub>4</sub>NO<sub>3</sub> is impacted by weather conditions such as temperature and relative humidity. Cheng et al. (2021) found that at high temperature and low relative humidity, NH<sub>4</sub>NO<sub>3</sub> may decompose into gas-phase NH<sub>3</sub> and HNO<sub>3</sub> allowing SO<sub>4</sub><sup>-2</sup> to be the dominant anion in the formation of iPM<sub>2.5</sub> during the summer. Local meteorological conditions also influence the equilibrium state. Walker et al., (2006) found that at both high and low relative humidity, NO<sub>3</sub><sup>-</sup> concentrations were inversely correlated with temperature. The formation of (NH<sub>4</sub>)<sub>2</sub>SO<sub>4</sub> is favored when temperatures are high and relative humidity is low, while NH<sub>4</sub>NO<sub>3</sub> is favored at low temperature and high relative humidity (Dawson et al., 2007). Since the gas-particle partitioning is affected by changes in ambient conditions, the partitioning will have seasonal variation. Higher temperature, relative humidity, and solar radiation favors the formation of iPM<sub>2.5</sub>; therefore, concentrations of PM<sub>2.5</sub>, SO<sub>4</sub><sup>-2</sup>, and NH<sub>4</sub><sup>+</sup> are higher in the summer than the winter in southeastern U.S. (Cheng et al., 2019a; Li et al., 2014a). Atmospheric H<sub>2</sub>SO<sub>4</sub> and HNO<sub>3</sub> form from the reactions shown in Equations 1.8 and 1.9.



In the equations above, SO<sub>2</sub> and NO<sub>x</sub> (NO<sub>2</sub> + NO + NO<sub>y</sub>) originate from anthropogenic emissions such as fossil fuel burning by power plants and industrial facilities, and exhaust emissions from vehicles and farm equipment. Agricultural soil is also a contributor for NO<sub>x</sub> emissions. In California, agricultural soil is a dominant source of NO<sub>x</sub> pollution where emissions are primarily controlled by soil moisture, inorganic nitrogen concentrations, and temperature (Almaraz et al., 2017; Sharon et al., 1996). NO<sub>x</sub> is generally represented by NO<sub>2</sub> and NO of

which  $\text{NO}_2$  is used for regulation. Although,  $\text{NO}$  is also plentiful in  $\text{NO}_x$ ; however, since it is rapidly converted into  $\text{NO}_2$ , it is not always accounted for (EPA 1999). The reactions in Equations 1.8 and 1.9 are photochemically driven, so both gases have short atmospheric life times of  $19 \pm 7$  hours (hr) in the summer and  $58 \pm 20$  hr in the winter for  $\text{SO}_2$ , and  $3.8 \pm 1.0$  hr for  $\text{NO}_x$  (Lee et al., 2011; Liu et al., 2016). Since  $\text{HNO}_3$  has a low photolysis rate in the lower atmosphere, it serves as a sink for  $\text{NO}_x$  (EPA 1979).

In comparison to  $\text{NH}_3$ ,  $\text{NH}_4^+$  has a much slower deposition velocity of 0.2 cm/s reported by Asman et al. (1998). While  $\text{NH}_3$  has a high deposition velocity, low source height, and short residence time,  $\text{NH}_4^+$  will deposit further downwind from its source due to a longer atmospheric residence time of 1-15 days (Phillips et al., 2004).  $\text{NH}_4^+$  is commonly deposited into the environment through wet deposition rather than dry. The wet deposition occurs when  $\text{NH}_4^+$  mixes into the clouds to form cloud droplets. Aerosol (gas + liquid) particles can act as a cloud condensation nucleus, where water droplets will aggregate on the aerosol surface and convert into cloud droplets. When these droplets form, they can absorb gaseous  $\text{NH}_3$ . The cloud-water is usually acidic, so most of the  $\text{NH}_3$  that is taken up by the drops will react with  $\text{H}^+$  to form  $\text{NH}_4^+$  (Asman et al., 1998).  $\text{iPM}_{2.5}$  that directly enters soils can alter plant growth or yield by affecting nutrient cycling, specifically nitrogen cycling, through its impacts on bacteria and fungi in the rhizosphere (Grantz et al., 2003). Asman & Jensen, (1993) found through model results that of total wet deposition of  $\text{NH}_x$ , 15% is from in-cloud scavenging of  $\text{NH}_3$ , 77% is from in-cloud scavenging of  $\text{NH}_4^+$ , 6% is from below-cloud scavenging of  $\text{NH}_3$  and 2% from below-cloud scavenging of  $\text{NH}_4^+$ .

### 1.2.3 Atmospheric Chemical Conditions and *iPM*<sub>2.5</sub> formation potential

In the literature, five chemical parameters were used to evaluate atmospheric chemical conditions and associated potential effects of NH<sub>3</sub> on *iPM*<sub>2.5</sub> formation (Cheng et al., 2019a, 2020; Seinfeld and Pandis, 1998; Wu et al., 2007; Makar et al., 2009).

The first chemical parameter is the gas ratio (GR), which describes the neutralization potential of NH<sub>3</sub>. When GR < 0, it indicates that there is an insufficient amount of NH<sub>3</sub> to neutralize all SO<sub>4</sub><sup>2-</sup>. When 0 < GR < 1, it indicates that there is sufficient NH<sub>3</sub> to neutralize SO<sub>4</sub><sup>2-</sup>, but not NO<sub>3</sub><sup>-</sup>. When GR > 1, it indicates NH<sub>3</sub>-rich conditions and that there will be sufficient supply to neutralize all SO<sub>4</sub><sup>2-</sup> and NO<sub>3</sub><sup>-</sup>. The GR is shown in Equation 1.10:

$$GR = \frac{[TA]-2[TS]}{[TN]} \quad (1.10)$$

Where [TA] is the total ammonia concentration (μmol/m<sup>3</sup>), the sum of [NH<sub>3</sub>] and [NH<sub>4</sub><sup>+</sup>]. [TS] is the total sulfate concentration (μmol/m<sup>3</sup>), the sum of [SO<sub>4</sub><sup>2-</sup>], [HSO<sub>4</sub><sup>-</sup>], and [H<sub>2</sub>SO<sub>4</sub>]. [TN] is the total nitrate concentration (μmol/m<sup>3</sup>), the sum of [NO<sub>3</sub><sup>-</sup>] and [HNO<sub>3</sub>]. According to Wu et al. (2007), NH<sub>3</sub> may not be fully neutralized by SO<sub>4</sub><sup>2-</sup> in winter conditions, so a more generic term should be used to account for neutralization by NO<sub>3</sub><sup>-</sup> such that an adjusted GR (AdjGR) should be used to examine *iPM*<sub>2.5</sub> sensitivity to NH<sub>3</sub> concentration. The AdjGR is shown in Equation 1.11:

$$AdjGR = \frac{[NH_3]+[NO_3^-]}{[TN]} \quad (1.11)$$

The second parameter is the particle neutralization ratio (PNR), which can identify if the secondary *iPM*<sub>2.5</sub> formed is NH<sub>3</sub> related. At a PNR ratio equal to 1, *iPM*<sub>2.5</sub> will be saturated with NH<sub>3</sub>, therefore, major reductions in ambient NH<sub>3</sub> would need to be made to reduce *iPM*<sub>2.5</sub>. When

the PNR ratio is  $< 1$ , then  $\text{NH}_3$  is limited and small reductions can reduce  $\text{iPM}_{2.5}$ . The PNR is shown in Equation 1.12:

$$\text{PNR} = \frac{[\text{NH}_4^+]}{2[\text{SO}_4^{2-}] + [\text{NO}_3^-]} \quad (1.12)$$

The third parameter is the mole ratio of total ammonia ( $\text{NH}_3 + \text{NH}_4^+$  particulate) to particulate sulfate ratio (TA/TS), which identifies if ambient conditions are acidic. When the ratio is  $< 1$  then the conditions are acidic and both  $(\text{NH}_4)_2\text{SO}_4$  and  $\text{H}_2\text{SO}_4$  will exist in the particle phase. A ratio between 1 and 2 indicates intermediate acidity and  $(\text{NH}_4)_2\text{SO}_4$ ,  $(\text{NH}_4)_2\text{HSO}_4$ , and  $(\text{NH}_4)_3\text{H}(\text{SO}_4)_2$  exist in the particle phase. When the ratio is  $> 2$  then the conditions are less acidic and  $(\text{NH}_4)_2\text{SO}_4$  and  $\text{NH}_4\text{NO}_3$  may exist in the particle phase depending on availability of  $\text{H}_2\text{SO}_4$  and  $\text{HNO}_3$ , and temperature. The TA/TS ratio is shown in Equation 1.13:

$$\text{TA/TS} = \frac{([\text{NH}_4^+] + [\text{NH}_3])}{[\text{SO}_4^{2-}]} \quad (1.13)$$

The fourth parameter is the gas-phase ammonia molar fraction ratio ( $\text{NH}_3/\text{NH}_x$ ), which defines if total  $\text{NH}_3$  primarily exists in the gas phase or particle phase. When the ratio is closer to zero, it indicates that  $\text{NH}_3$  is neutralized by  $\text{H}_2\text{SO}_4$  and/or  $\text{HNO}_3$  and converted to  $\text{NH}_4^+$ . When the ratio is close to 1, there is excessive un-neutralized  $\text{NH}_3$  in the gas phase. When  $\text{NH}_3/\text{NH}_x$  is equal to 0.5, there is an equal amount of  $\text{NH}_3$  in the gas phase and  $\text{NH}_4^+$  in the particle phase.

The  $\text{NH}_3/\text{NH}_x$  ratio is shown in Equation 1.14:

$$\text{NH}_3/\text{NH}_x = \frac{[\text{NH}_3]}{[\text{NH}_3] + [\text{NH}_4^+]} \quad (1.14)$$

The final parameter is the fraction of ammonia sensitive  $\text{iPM}_{2.5}$  (AN) to total  $\text{PM}_{2.5}$ , which quantifies the mass fraction of  $\text{PM}_{2.5}$  that is directly sensitive to changes in  $\text{NH}_3$

emissions. When AN/PM<sub>2.5</sub> approaches 1, PM<sub>2.5</sub> is more sensitive to NH<sub>3</sub> while AN/PM<sub>2.5</sub> closer to 0 indicates insensitivity. This parameter is shown in Equation 1.15:

$$\text{AN/PM}_{2.5} = \frac{([\text{NH}_4^+] + [\text{NO}_3^-])}{[\text{PM}_{2.5}]} \quad (1.15)$$

#### ***1.2.4 Thermodynamic Equilibrium Modeling***

Understanding the gas-particle partitioning will help bridge the knowledge gap of the behavior of secondary PM<sub>2.5</sub> formation influenced by agricultural NH<sub>3</sub> emissions; however, calculations can be quite complex. The gas-particle partitioning is assumed to be in thermodynamic equilibrium (Xu et al., 2020), so modeling of this equilibrium can be a useful method to calculate the composition and phase state of aerosols. The ISORROPIA-II is a commonly used thermodynamic equilibrium model for multiphase multicomponent inorganic aerosol, it simulates the dynamics of phase changes and interaction of different chemical species including NH<sub>4</sub><sup>+</sup>, NO<sub>3</sub><sup>-</sup>, SO<sub>4</sub><sup>2-</sup>, Cl<sup>-</sup>, K<sup>+</sup>, Ca<sup>+2</sup>, Mg<sup>+2</sup>, Na<sup>+</sup> in ambient PM<sub>2.5</sub> (Cheng et al., 2021). These species are in thermodynamic equilibrium with atmospheric gases and humidity, and so it is important to select a model that can account for them. The original version, ISORROPIA, was developed at the University of Miami, and the ISORROPIA-II version was later developed at the Georgia Institute of Technology. The ISORROPIA model is computationally efficient, which has made it the model of choice for thermodynamic equilibrium calculations in three-dimensional air quality models such as CMAQ and GEOS-Chem (Fountoukis and Nenes, 2007). The ISORROPIA-II model adds the thermodynamics of the crustal species into an already pre-existing model, which has previously been a limitation to other thermodynamic equilibrium models (Fountoukis and Nenes, 2007). The model runs under one of two thermodynamic states: the stable state, where the model assumes salts precipitate when super saturation occurs, and the metastable state, where the model assumes salts remain in the aqueous phase. ISORROPIA-II

can solve for the forward problem, in which measured values of temperature, relative humidity, total (gas + aerosol) concentrations of  $\text{NH}_3$  and  $\text{NO}_3^-$ , and aerosol  $\text{SO}_4^{-2}$  concentration are used to calculate the gas concentrations,  $\text{iPM}_{2.5}$ , water content, and  $\text{H}^+$ . The model can also solve the reverse problem, in which known quantities of temperature, relative humidity and aerosol concentrations of  $\text{NH}_3$ ,  $\text{SO}_4^{-2}$ ,  $\text{NO}_3^-$  are used to solve the partitioning of  $\text{NH}_3\text{-NH}_4^+$ . Due to the rapid reactivity of  $\text{H}_2\text{SO}_4$ , ISOROPPIA-II assumes that all  $\text{SO}_4^{-2}$  exists in the particle phase. The model considers important thermodynamic factors such as equilibrium constants, activity of species, activity coefficients, aerosol water content, deliquescence relative humidity, and mutual deliquescence relative humidity when solving for the gas-particle partitioning of  $\text{NH}_3\text{-NH}_4^+$ .

The thermodynamic equilibrium is assumed to be established instantaneously by ISOROPPIA-II. However, equilibrium can be achieved within a few minutes for submicron particles ( $\text{PM}_1$ ), often faster with changes in ambient conditions, while coarse particles ( $\text{PM}_{2.5-10}$ ) require more time, on the order of one hour or more (Meng and Seinfeld, 1996). Therefore, if ambient conditions and inorganic aerosol compositions are variable on timescales shorter than the sampling timescale, then that could be problematic for an equilibrium model application (Cheng et al., 2022). In addition, organic matter can cause a significant impact on the time that it takes to achieve equilibrium. Liggio et al., (2011) found that  $\text{NH}_3$  neutralized acidic aerosols < 1 min in organic free air, but the time increased to between 10 min to several hours in the presence of organic gases. Silvern et al., (2017) also found low  $\text{NH}_4^+/\text{SO}_4^{-2}$  ratio in the summer time in Southeastern US despite excess ambient  $\text{NH}_3$ , which was possibly due to organic matter coating the  $\text{SO}_4^{-2}$  particles, limiting the reacting with  $\text{NH}_3$ . This theory was further tested in the same region by others (Cheng et al., 2022; Guo et al., 2018), who found that  $\text{NH}_3$  uptake was not affected by organic aerosol content but suggested that further testing with higher data resolution

and in a different region should be conducted. Despite the instantaneous equilibrium assumption, the non-equilibrium state could still exist due to heterogeneous surfaces, differences in particle sizes, and equilibrium time for particles with a diameter  $> 1 \mu\text{m}$  (Ravishankara, 1997; Wexler and Seinfeld, 1992; Moya et al., 2002), so modeling under certain ambient conditions could lead to incorrect predictions.

Performance of the model with 24 hr data from urban and suburban sites was analyzed by Cheng et al. (2022). It was discovered when temperature was  $>10 \text{ }^\circ\text{C}$  and relative humidity  $< 60\%$ , the model overpredicted  $\text{HNO}_3$  and underpredicted  $\text{NO}_3^-$  concentrations. Performance under metastable and stable setups showed no difference at higher relative humidity ( $\text{RH} > 83\%$ ) and low temperature ( $T < 5 \text{ }^\circ\text{C}$ ). When comparing the metastable state and stable state settings, the metastable state could perform better when temperature  $> 10 \text{ }^\circ\text{C}$  and relative humidity  $< 60\%$ , while the stable state could perform better when temperature  $< 5 \text{ }^\circ\text{C}$ . In regions where  $\text{SO}_4^{2-}$  is not the dominant particle in  $\text{iPM}_{2.5}$ , the performance may vary. The model was also used by Li et al., (2014a) to simulate  $\text{iPM}_{2.5}$  in response to  $\text{NH}_3$  emissions from an egg production facility in Southeastern US, they reported a good agreement in predicting  $\text{NH}_4^+$  and  $\text{NO}_3^-$  concentrations at ambient stations. However, ISORROPIA-II predicted most of total  $\text{Cl}^-$  (gas + aerosol) to be partitioned in the gas phase, potentially due to low measured Cl concentrations.

## **1.3 RESEARCH GAPS AND HYPOTHESIS**

### ***1.3.1 Research Gaps***

Through the aforementioned literature review, the following research gaps were identified:

- 1) Although transformation of atmospheric  $\text{NH}_3$  has been well studied and understood, very limited research was conducted to advance our understanding of the dynamics of such

transformation in animal feeding operations (AFOs) environments, where ambient  $\text{NH}_3$  concentration may be rich and yet availability of acidic pollutant gases may be limited.

- 2) Gas-particle partitioning of  $\text{NH}_3\text{-NH}_4^+$  as impacted by AFOs emissions (organic and inorganic pollutants) is not well understood.

### ***1.3.2 Research hypothesis***

Although  $\text{NH}_3$  emissions from AFOs cause overly rich ambient  $\text{NH}_3$  concentration in rural areas, limited availability of acidic gases alters atmospheric chemical conditions and leads to limited formation of secondary  $\text{iPM}_{2.5}$  as impacted by AFO  $\text{NH}_3$  emissions under various meteorological conditions.

## **1.4 RESEARCH OBJECTIVES**

The ultimate goal of this project was to assess formation of secondary  $\text{iPM}_{2.5}$  as impacted by the ambient  $\text{NH}_3$  concentration in proximity to an AFO. To reach this goal, the project aimed to fulfill the following supporting objectives:

- 1) Investigate  $\text{iPM}_{2.5}$  precursor gas (i.e.  $\text{NH}_3$ ,  $\text{SO}_2$ ,  $\text{NO}_x$ ) concentrations and  $\text{iPM}_{2.5}$  concentration in the vicinity of a poultry production facility
- 2) Investigate atmospheric chemical conditions under various meteorological conditions
- 3) Estimate  $\text{NH}_3$  neutralization potential, gas-particle partitioning of  $\text{NH}_3$  gas and  $\text{NH}_4^+$  particle for prediction of  $\text{iPM}_{2.5}$  formation as impacted by atmospheric chemical and meteorological conditions in a poultry production environment

## CHAPTER 2: METHODOLOGY

### 2.1. RESEARCH SITE

#### 2.1.1 *The Poultry Production Unit*

As of 2021, North Carolina (NC) ranked 4<sup>th</sup> in broiler production, 2<sup>nd</sup> in turkey production, 8<sup>th</sup> in egg production, and 3<sup>rd</sup> in swine production in the US with approximate 67,000 poultry and swine production farms across the state (Dietrich, 2019). The study of AFO NH<sub>3</sub> emissions impacts on the formation of secondary iPM<sub>2.5</sub> in NC will provide good implications of the impacts nationally, therefore, this study was conducted at the Poultry Unit of the NC Department of Agriculture (NCDA) Piedmont Research Station, located in Salisbury, NC as shown in Figure 2.1. The site is approximately 4.70 and 20.88 km away from the Rowan and Duke Energy power plants, respectively, both of which are natural gas combined-cycle power plants.

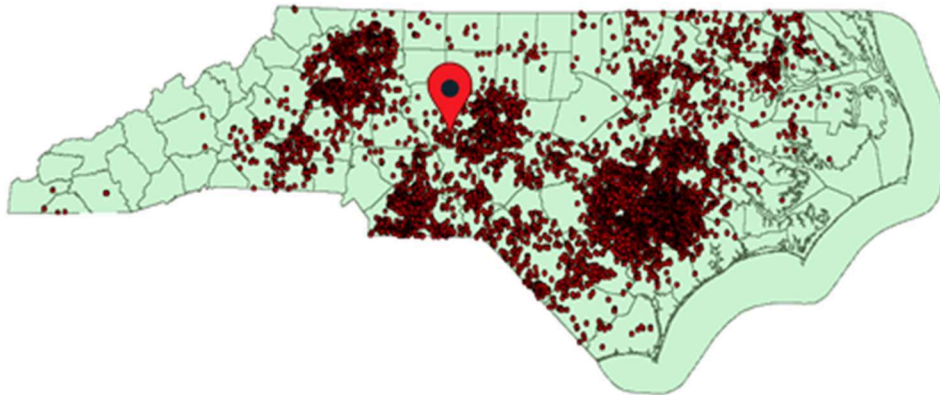


**Figure 2.1. Spatial distribution of poultry & swine farms in NC (Dietrich, 2019) and the research site location**

As shown in Figure 2.2, the Poultry Unit has eight mechanically ventilated poultry houses, a free-range pasture for egg layers, and a manure shed. The poultry houses can hold 15,000 commercial laying hens, 8,000 broiler breeders, and incubators with around 52,000 eggs

hatching at a time. Field crops (mainly forages, corn, and soybeans) around the houses are produced in a continuous no-till cropping system. When there is no land application of manure, the poultry houses and manure storage shed are the sources of  $\text{NH}_3$ . The  $\text{PM}_{2.5}$  emissions may come from poultry houses, on farm vehicles, or other farming operations. Due to the adverse impact by the COVID-19 pandemic, poultry population on the farm was significantly reduced leading to low  $\text{NH}_3$  emission and ambient concentrations.

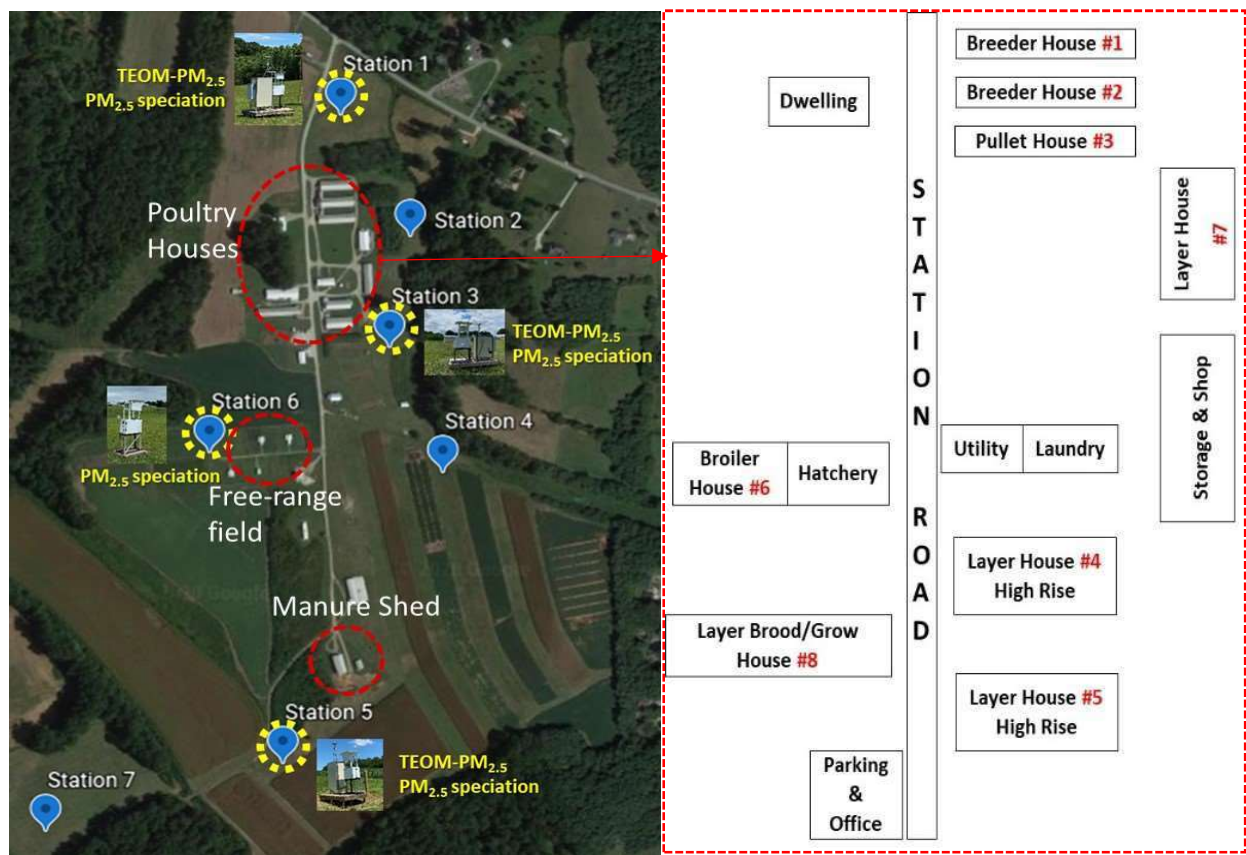


Figure 2.2. Research site layout and the ambient air monitoring and sampling stations

### 2.1.2 Ambient Air Monitoring and Sampling Stations

The site contains seven stations for air monitoring and sampling shown in Figure 2.2 under an NSF funded project “Fate, Transport and Transformation of  $\text{NH}_3$  Emissions from AFOs and Their Impacts on Air-Soil Health”. Stations 1, 3, 5, and 6 (i.e., ST1, ST3, ST5, ST6) were

used for this particular study, which is a sub-project of the NSF project. Stations 1, 3, and 5 each contained a Partisol Model 2300 Chemical Speciation Sampler for PM<sub>2.5</sub> chemical composition measurements, Ogawa passive samplers for precursor gases (i.e., NH<sub>3</sub>, SO<sub>2</sub> and NO<sub>2</sub>) measurements, and a tapered element oscillating microbalance (TEOM) used for ambient PM<sub>2.5</sub> concentrations measurements. Each of the TEOM samplers were equipped with a PM<sub>10</sub> and a PM<sub>2.5</sub> sampler heads for continuous measurements of ambient PM<sub>2.5</sub> concentrations. Station 6 only contained a Partisol Model 2300 Chemical Speciation Sampler and Ogawa passive samplers. The location for each station was selected to account for all wind directions, so that at least one station would be downwind from one of the sources at all times.

## **2.2. PM<sub>2.5</sub> CHEMICAL SPECIATION SAMPLING AND PRECURSOR GASES SAMPLING**

### ***2.2.1 PM<sub>2.5</sub> Chemical Speciation Sampling Method***

Partisol Model 2300 chemical speciation samplers were used to take PM<sub>2.5</sub> samples for the full spectrum of chemical speciation. The instrument contained four flow channels capable of operating at varying flow rates. Each channel was equipped with a PM<sub>2.5</sub> cartridge. The PM<sub>2.5</sub> cartridge was made of three components: (1) an impactor (a.k.a. PM<sub>2.5</sub> inlet) with a cut-off size of 2.5 μm to remove particles >2.5 μm, (2) slot for a honeycomb denuder to remove gas phase NH<sub>3</sub> when coated with acid solution, and (3) a filter holder. Figure 2.3 illustrates the sampler and the filter cartridge assembly.



**Figure 2.3. Partisol speciation sampler (left) and filter cartridges (right)**

Figure 2.4 illustrates the flow schematic of Partisol PM<sub>2.5</sub> speciation sampler. The first channel operated at a flow rate of 16.7 L/min and used a Teflon filter (2.0 μm pore size, 47mm) to capture the mass of PM<sub>2.5</sub> for mass concentration and elemental analysis. The second channel operated at a 10 L/min flow rate and was equipped with a honeycomb denuder coated with 2% citric acid in ethanol to capture gaseous NH<sub>3</sub> in the sampled air as it passed through the denuder. The denuder collects up to 12mg NH<sub>3</sub> with high collection efficiency (99.9%) when NH<sub>3</sub> concentration is low (Li et al. 2014b). A nylon filter (0.2 μm pore size, 47 mm) was placed down-stream of the honeycomb denuder to capture PM<sub>2.5</sub> for particle phase ion (i.e., anions and cations) analyses. Spacers were also placed around the honeycomb denuder to avoid contact with the cartridge. The third channel operated at 16.7 L/min and used a quartz filter (47mm) to capture PM<sub>2.5</sub> for OC/EC analyses. Finally, the fourth channel is typically used as a field blank sample, but was not utilized for this project. The sampling time of the Partisol sampler was 24 hr for each event.

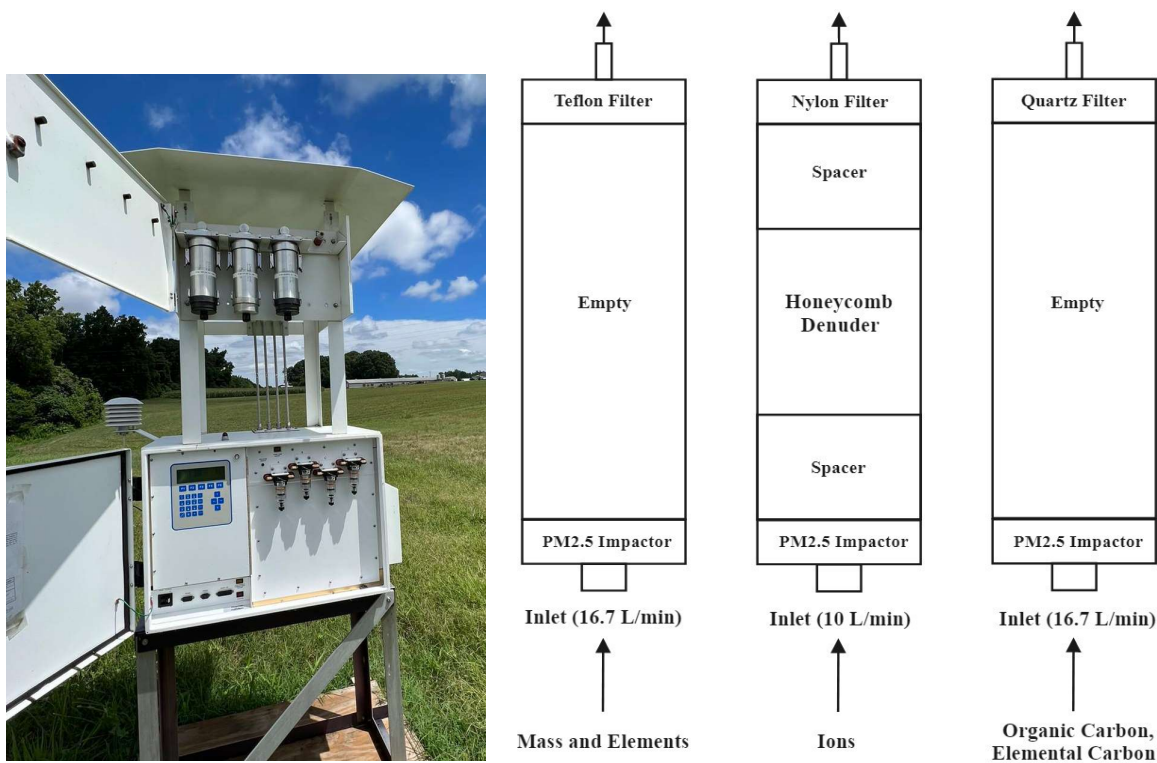


Figure 2.4. Partisol PM<sub>2.5</sub> speciation sampler in the field (left) and its flow schematic (right)

### 2.2.2 Precursor Gases Sampling Methods

Since the research site is located in a rural environment, ambient concentrations of SO<sub>2</sub> and NO<sub>2</sub> were expected to be low, the Ogawa passive sampler were selected and co-located with the Partisol PM<sub>2.5</sub> speciation samplers to take air samples for SO<sub>2</sub> and NO<sub>2</sub> concentration determination. This type of passive sampler detection limit was 2.3 ppb to 0.3 ppb for a 1 day to 14 day duration, respectively (Site). Based upon previous air sampling experience by the collaborators at Research Triangle International (RTI), the passive samplers were deployed for up to 14 days while PM<sub>2.5</sub> speciation sampling was occurring. Gas-phase NH<sub>3</sub> was also captured with the passive samplers to compare the measurements of NH<sub>3</sub> concentrations with the honeycomb denuder in the speciation samplers.

The passive samplers capture ambient gases through diffusion by using collection pads coated with an absorption reagent. Diffusion, molecules moving from a higher concentration to a lower concentration, can be defined by Fick's first law shown in Equation 2.1:

$$D = - \frac{J}{c_1 - c_2 / Z} \quad (2.1)$$

Where, D is the diffusion coefficient in  $\text{cm}^2/\text{s}$ , J is the flux in  $\text{g}/\text{cm}^2\text{-s}$ ,  $c_1$  is the higher concentration in  $\text{g}/\text{m}^3$ ,  $c_2$  is the lower concentration in  $\text{g}/\text{m}^3$ , and l is the length in m. To capture  $\text{SO}_2$  and  $\text{NO}_2$ , the pads were coated with triethanolamine, and for  $\text{NH}_3$ , the pads were coated in citric acid. The details of the Ogawa passive sampler are shown in Figure 2.5.

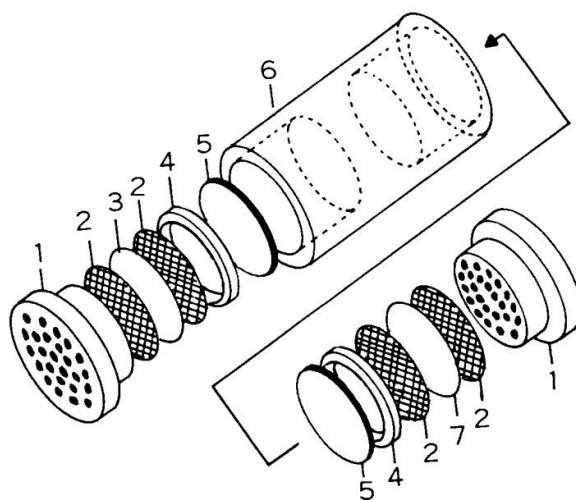


**Figure 2.5. Details of Ogawa passive sampler (Ogawa USA 2006)**

The components of the sampler include (1) diffuser end caps, (2) stainless screens, (3, 7) collection pad, (4) Teflon ring, (5) Teflon disc, and (6) sampler body. Station 1, 3, 5, and 6 were equipped with duplicates of each sampler; one sampler with a pad to capture  $\text{SO}_2/\text{NO}_2$  on one end and a pad to capture  $\text{NO}_x$  on the other end, and another sampler with  $\text{NH}_3$  collection pads on both sides of the passive sampler. Blanks were also collected to measure background levels for

each precursor gas and subtracted from field samples. Samples were deployed between 1.5 m to 2 m off the ground.

### **2.2.3 Sampling Preparation**

All samples were handled using nitrile gloves and were prepared in a clean air lab. Honeycomb denuders were cleaned with deionized water before application of citric acid. Figure 2.6 shows the application of citric acid to the honeycomb denuder. The 2% citric acid solution was applied to each perforated hole, and both ends of the denuder were covered with red caps and then inverted a few times to ensure an even coating of the solution. All denuders were coated a day before their respective sampling event.



**Figure 2.6. Application of 2% citric acid solution to coat honeycomb denuders**

Nylon and quartz filters were placed in petri dishes and grouped together in Ziploc bags, shown in Figure 2.7. Teflon filters were conditioned before and after sampling for a minimum of 24 hours in controlled conditions at 20°C–30°C with less than  $\pm 2^\circ\text{C}$  variation and 30–40% RH with less than  $\pm 5\%$  variation. The filters were weighed on an analytical balance with a readability of  $\pm 1\mu\text{g}$  following 40CFR, Part 50 (CFR, Wang-Li, 2013). The Teflon filters were conditioned and weighed pre-sampling and post sampling at the aerosol laboratory of RTI at

Research Triangle Park (RTP), NC. The pre-weighed Teflon filters were kept in petri dishes and placed individually in their own bags to protect them from contamination.

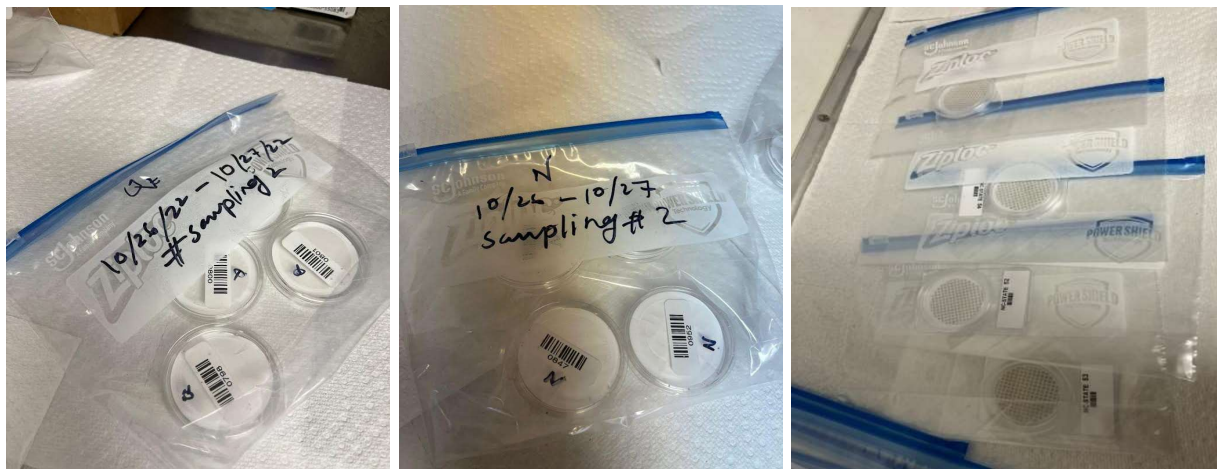


**Figure 2.7. Storage of quartz (left), nylon (middle), and Teflon (right) filters for transporting to the field**

Passive samplers were assembled on a clean surface using tweezers shown in Figure 2.8. Once each sample was assembled, they were placed in their own Ziploc bag and airtight storage container, shown in Figure 2.8. All samples were barcoded for identification.



**Figure 2.8. Assembling passive samplers (left) and Ogawa airtight storage container (right)**

### 2.2.4 Sampling in the Field

Upon arrival at the research site, filters and denuders were removed from their Ziploc bags and placed in their respective cartridges (Figure 2.9) in the research trailer (a.k.a. mobile lab). Each cartridge was labeled which station they were going to be deployed at.



**Figure 2.9. Installing filters to the cartridges in the field mobile lab**

The procedure for setting up and running the Partisol Chemical Speciation Sampler for all stations was followed using the instrument's operating manual. Upon arrival at the station, the sampler was powered on, and all previous stored data and settings were reset. The current time and date, sampling duration (24 hr), and sampling start time were entered on the sampler display screen. The flow rate for each flow channel was set to 16.7, 10, 16.7, and 0 L/min for channels A, B, C, and D, respectively. The PM<sub>2.5</sub> cartridges were placed on the cartridge mount shown in Figure 2.10. The samplers were put on standby mode and the end caps were removed from the PM<sub>2.5</sub> cartridges. Once the starting time arrived, the sampler would then go into sampling mode and run for the set duration time of 24 hours. Once 24 hours had passed, the sampler stopped all flow and entered standby mode until further input was made.



**Figure 2.10. Illustration of PM<sub>2.5</sub> speciation samplers (left), co-located samplers (middle), Ogawa passive samplers with replicates (right)**

The Ogawa passive samplers were removed from their storage vials and Ziploc bags. The samplers were placed on Velcro strips to be mounted inside a black container shown in Figure 2.10. Duplicates for each precursor gases were deployed at each station.

### ***2.2.5 PM<sub>2.5</sub> and Precursor Gases Sampling Schedule***

The PM<sub>2.5</sub> samples were simultaneously taken at ST1, ST3, ST5, and ST6 from July 11-December 13, 2022, covering three seasons with 10 sampling events in summer, 3 events in autumn and 7 events in winter. The passive samplers were deployed between 6 to 14 days throughout the entire sampling period since ambient concentrations of HNO<sub>3</sub> and H<sub>2</sub>SO<sub>4</sub>, converted from NO<sub>2</sub> and SO<sub>2</sub>, respectively, were expected to be low in the rural environment. A summary of the sampling events is provided in Table 2.1.

**Table 2.1. Sampling event summary**

Event	PM <sub>2.5</sub> Spectrum Sampling		Passive Sampling		Season	Bird* Population
	Start Date	End Date	Start Date	End Date		
1	7/11/2022	7/12/2022				1366
2	7/12/2022	7/13/2022	7/11/2022	7/25/2022	Summer	1366
3	8/12/2022	8/13/2022				1366
4	8/13/2022	8/14/2022				1366
5	8/14/2022	8/15/2022				1366
6	8/17/2022	8/18/2022				1366
7	8/18/2022	8/19/2022				1366
8	8/23/2022	8/24/2022	8/12/2022	8/26/2022	Summer	1366
9	8/24/2022	8/25/2022				1366
10	8/25/2022	8/26/2022				1366
11	10/25/2022	10/26/2022				1362
12	10/26/2022	10/27/2022	10/25/2022	11/08/2022	Autumn	1361
13	10/27/2022	10/28/2022				1361
14	11/16/2022	11/17/2022				1355
15	11/17/2022	11/18/2022	11/16/2022	12/01/2022	Winter	1355
16	11/18/2022	11/19/2022				1355
17	12/10/2022	12/11/2022				1355
18	12/11/2022	12/12/2022				1355
19	12/12/2022	12/13/2022	12/10/2022	12/16/2022	Winter	1355
20	12/13/2022	12/14/2022				1355

\*birds were housed in production house 7 during sampling events

### 2.2.6 Post Sampling

After completion of each sampling event, all cartridges were removed from the speciation samplers and taken to the on-site mobile lab for extraction. Filters were taken from the cartridges and placed back in their own petri dishes, labeled with a barcode. All petri dishes with quartz filters were grouped together and placed into a Ziploc bag. Petri dishes with nylon filters were also grouped together and placed into their own Ziploc bags. Petri dishes with Teflon filters remained separated and were placed in their own respective Ziploc bags. All filters were

transported in a cooler with dry ice from the research site and temporarily stored in a refrigerator. Honeycomb denuders were taken out from the denuder/nylon filter cartridge, capped at both ends and placed in a Ziploc bag to be transported to the research lab in a cooler. After completion of each passive sampling event, each passive sampler was placed in its own Ziploc bag and stored in the Ogawa airtight storage container. The storage containers were labeled with a barcode for location identification.

Upon returning from the site, the  $\text{NH}_3$  collected by the honeycomb denuder was extracted using 15 mL deionized (DI) water and placed into a vial (Figure 2.11) to be stored in the refrigerator. Teflon, nylon filters, denuder extraction vials, and passive sampling storage containers were transported to the RTI at RTP, NC after completion of each of seasonal sampling events for chemical analysis described in section 2.4. Quartz filters were placed into the freezer until OC/EC analyses.



**Figure 2.11. Storage of filters and denuders for transportation (left) and denuder samples after extraction in vials (right)**

### ***2.3. Meteorological Data Collection***

Meteorological data were collected from a weather station located one mile from the research site. Weather data source may be found at <https://products.climate.ncsu.edu/cardinal/scout/?station=SALI>. Table 2.2 lists the ambient temperature, relative humidity (RH), wind speed, and wind direction at the research site on the sampling dates. Each variable was calculated using hourly data from the start time to end time for each sampling event. In summer, the sampling ST1 was at the prevailing downwind of the farm, whereas ST6 was at prevailing upwind of the farm. In autumn, ST1 was at the prevailing downwind two out of three sampling events, whereas in winter, almost half of the time, ST1 was not at the prevailing downwind location. During all the sampling events, the mean wind speeds were in the ranges of  $0.52 \pm 0.38$  to  $1.73 \pm 1.13$  m/s; therefore, the research observations may not apply to windy day scenarios.

**Table 2.2. Meteorological data at the research site**

Start Date	Ambient Temperature (K)	Ambient RH (%)	Wind Speed (m/s)	Prevailing Wind
11 Jul 2022	297.44 ± 3.21	79.29 ± 16.34	0.89 ± 0.68	SW
12 Jul 2022	300.26 ± 3.44	75.74 ± 16.77	1.30 ± 1.00	SW
12 Aug 2022	295.09 ± 4.32	78.76 ± 17.23	1.16 ± 0.94	SE
13 Aug 2022	295.25 ± 4.98	69.48 ± 25.82	0.88 ± 0.89	S
14 Aug 2022	295.42 ± 3.44	82.48 ± 16.35	1.30 ± 0.86	SE
17 Aug 2022	295.60 ± 2.54	82.62 ± 15.78	0.97 ± 0.86	S
18 Aug 2022	296.50 ± 3.46	79.81 ± 15.57	0.62 ± 0.56	SE
23 Aug 2022	296.53 ± 4.51	82.06 ± 17.68	0.69 ± 1.05	S
24 Aug 2022	297.51 ± 3.75	84.16 ± 18.39	0.57 ± 0.52	S
25 Aug 2022	296.82 ± 3.68	84.88 ± 14.19	0.66 ± 0.47	SW
25 Oct 2022	289.13 ± 4.30	76.25 ± 23.35	0.78 ± 0.92	S
26 Oct 2022	287.23 ± 3.77	71.57 ± 10.78	1.60 ± 1.28	SW
27 Oct 2022	285.30 ± 3.99	70.15 ± 16.20	1.65 ± 1.09	E
16 Nov 2022	278.07 ± 4.87	73.03 ± 16.38	1.73 ± 1.13	W
17 Nov 2022	274.07 ± 5.08	71.23 ± 27.32	0.78 ± 0.81	SW
18 Nov 2022	276.48 ± 4.94	68.18 ± 26.82	0.81 ± 1.00	SW
10 Dec 2022	281.76 ± 1.06	78.45 ± 4.65	1.13 ± 0.54	E
11 Dec 2022	279.58 ± 3.60	88.27 ± 13.49	0.96 ± 0.88	S
12 Dec 2022	279.16 ± 3.82	75.61 ± 14.35	1.45 ± 1.19	E
13 Dec 2022	275.45 ± 3.05	84.47 ± 15.77	0.52 ± 0.38	SE

## 2.4. PM<sub>2.5</sub> CHEMICAL SPECIATION AND PASSIVE GAS SAMPLE ANALYSES

### 2.4.1 PM<sub>2.5</sub> Chemical Speciation Analyses

PM<sub>2.5</sub> chemical speciation analyses include ions (anions and cations) from nylon filters, mass concentration and trace elements from Teflon filters, and OC/EC from Quartz filters (Wang-Li, 2013). Table 2.3 summarizes the chemical species along with corresponding analytical methods used for this research. The ionic and elemental analyses of the sampled PM<sub>2.5</sub> were conducted by the collaborators of RTI at RTP, NC, following standard operating

procedures (SOPs) for EPA’s National PM<sub>2.5</sub> Chemical Speciation Network (EPA, 2020). The OC/EC analyses were conducted at the Air Quality Laboratory in the Civil Engineering Department at NC State.

**Table 2.3. PM<sub>2.5</sub> chemical speciation species and methods**

Filter	Analytic method/equipment	Chemical species
Nylon	Ion chromatography (IC)	NH <sub>4</sub> <sup>+</sup> , Na <sup>+</sup> , and K <sup>+</sup> , NO <sub>3</sub> <sup>-</sup> , SO <sub>4</sub> <sup>2-</sup> , Cl <sup>-</sup>
	Gravimetric with microbalance	Mass concentration
Teflon	Energy dispersive X-ray fluorescence (EDXRF) spectrometry	Ag, Al, As, Ba, Br, Ca, Cd, Ce, Cl, Co, Cr, Cs, Cu, Fe, In, K, Mg, Mn, Na, Ni, P, Pb, Rb S, Sb, Se, Si, Sn, Sr, Ti, V, Zn, Zr
Quartz	Thermal-optical aerosol analyzer	OC, EC

For ionic analyses, particulate samples on the nylon filters were extracted using an ultrasonic bath into DI water in vials and were then analyzed by ion chromatography (IC) for major ions as listed in Table 2.3.

For mass and elemental analyses, Teflon filters were conditioned in an environmentally controlled filter weighing chamber for 24-48 hours and weighed by a microbalance with a minimum readability in ±1µg and a repeatability in 1µg. The energy dispersive X-ray fluorescence (EDXRF) spectrometry was used to determine 33 elements (Table 2.3) of particulate deposits on the Teflon filters.

For carbon species analyses, the analysis was done by a Thermal-Optical Aerosol Analyzer (Sunset Laboratory Inc. OR, US). A single 1 cm<sup>2</sup> punch of subsample was taken from a quartz filter and placed in the front oven of the analyzer. The sampler used a NIOSH-like method to calculate the OC and EC of the quartz filter subsample. The analyzer reports OC and EC

content in  $\mu\text{g}/\text{cm}^2$  (a.k.a. the sample density, D) on the filter punch. Then, the OC and EC mass loading on the filter, m, was calculated using Equation 2.2:

$$m = D * A \quad (2.2)$$

Where, D is the sample area density on the filter punch in  $\mu\text{g}/\text{cm}^2$ , and A is the area of the quartz filter ( $17.35 \text{ cm}^2$ ).

#### ***2.4.1 Precursor Gas Sample Analyses***

Denuder extraction and passive sampling pads were also analyzed at RTI by IC. The passive sampler collection pads were first removed from the sampler body and placed into an extraction vial with 8 mL of DI water. The collection pad in the vial was allowed to sit for 30 minutes with periodic shaking during the extraction period. The IC provided liquid mass concentration of  $\text{NH}_4^+$  of denuder extraction samples in vials, mass loading on passive pads for  $\text{SO}_2$  and  $\text{NO}_2$ , further calculations were done to convert (1) the mass concentration of  $\text{NH}_4^+$  in liquid to the mass concentration of  $\text{NH}_3$  in air, (2) mass loading of  $\text{SO}_2$  and  $\text{NO}_2$  to mass concentrations of  $\text{SO}_2$  and  $\text{NO}_2$  in the air.

### **2.5. $\text{PM}_{2.5}$ CHEMICAL SPECIES AND PRECURSOR GAS CONCENTRATION DETERMINATIONS**

#### ***2.5.1 Concentrations of $\text{PM}_{2.5}$ Chemical Species***

For the ionic species on the nylon filters, the IC provided measurements of mass concentrations in extraction liquid, therefore the ionic mass sampled on the nylon filter was calculated using Equation 2.3:

$$m_i = C_i * V \quad (2.3)$$

Where,  $m_i$  is the mass of individual ionic species ( $\text{NH}_4^+$ ,  $\text{Na}^+$ , and  $\text{K}^+$ ,  $\text{NO}_3^-$ ,  $\text{SO}_4^{2-}$ ,  $\text{Cl}^-$ ) in  $\mu\text{g}$ ,  $C_i$  mass concentration ( $\mu\text{g}/\text{m}^3$ ) of ionic species in DI water measured by IC, V is the volume

(m<sup>3</sup>) of DI water in extraction vials. The concentrations of ionic species in air were further calculated using Equation 2.4:

$$C_i = \frac{m_i}{Q_N \cdot t} \quad (2.4)$$

Where, C<sub>i</sub> is the concentrations of individual ionic species (NH<sub>4</sub><sup>+</sup>, Na<sup>+</sup>, and K<sup>+</sup>, NO<sub>3</sub><sup>-</sup>, SO<sub>4</sub><sup>-2</sup>, Cl<sup>-</sup>) in µg/m<sup>3</sup>, m<sub>i</sub> is the mass of individual ionic species, Q<sub>N</sub> is the air sampling flow rate through nylon filter cartridge (10 l/min=0.6 m<sup>3</sup>/hr); t is the sampling duration (24 hr) of each sampling event.

For PM<sub>2.5</sub> mass concentration from Teflon filters, it was calculated using Equation 2.5:

$$C_{PM_{2.5}} = \frac{m_2 - m_1}{Q \cdot t} \quad (2.5)$$

Where, C<sub>PM<sub>2.5</sub></sub> is the PM<sub>2.5</sub> mass concentration in µg/m<sup>3</sup>, m<sub>2</sub> is the weight of conditioned Teflon filter post sampling in µg; m<sub>1</sub> is the weight of conditioned Teflon filter prior to the sampling in µg, Q is the air sampling flow rate through Teflon filter cartridge (16.7 l/min=0.96 m<sup>3</sup>/hr); t is the sampling duration (24 hr) of each sampling event.

For the elemental species, the EDXRF spectrometry provided mass loading of each of the elements on the Teflon filters; therefore, the concentrations of the individual elements were calculated using Equation 2.6:

$$C_e = \frac{m_e}{Q_T \cdot t} \quad (2.6)$$

Where, C<sub>e</sub> is the mass concentration of individual elements in µg/m<sup>3</sup>, m is mass of individual elements on the filter in µg, Q<sub>T</sub> is the air sampling flow rate through Teflon filter cartridge (16.7 l/min=0.96 m<sup>3</sup>/hr); t is the sampling duration (24 hr) of each sampling event.

For carbon species, the concentrations of OC and EC in the air were calculated using Equation 2.7:

$$C_c = \frac{m}{Q_q * t} \quad (2.7)$$

Where,  $C_c$  is the mass concentration of OC or EC in  $\mu\text{g}/\text{m}^3$ ,  $m$  is the OC or EC mass loading (equation 2.2) in  $\mu\text{g}$ ,  $Q_q$  is the air sampling flow rate through quartz filter cartridge (16.7 l/min 0.96  $\text{m}^3/\text{hr}$ );  $t$  is the sampling duration (24 hr) of each sampling event.

### 2.5.2 $\text{NH}_3$ Concentration by Using Denuder

Using Equation 2.3,  $\text{NH}_4^+$  mass loading in denuder extraction,  $m_{\text{NH}_4^+}$  ( $\mu\text{g}$ ) was calculated from the IC analysis, this mass loading then was used to calculate  $\text{NH}_3$  concentration in the air by equation 2.8:

$$C_{\text{NH}_3} = \frac{m_{\text{NH}_4^+} * \text{MW}_{\text{NH}_3} / \text{MW}_{\text{NH}_4^+}}{Q_d * t} \quad (2.8)$$

Where,  $C_{\text{NH}_3}$  is the  $\text{NH}_3$  mass concentration in  $\mu\text{g}/\text{m}^3$ ,  $Q_d$  is the air sampling flow rate through the honeycomb denuder in cartridge) at 10 L/min (0.6  $\text{m}^3/\text{hr}$ ),  $\text{MW}$  is molecular weight in  $\mu\text{g}/\text{mol}$ , and  $t$  is the sampling duration (24 hr).

### 2.5.3 $\text{NH}_3$ , $\text{NO}_2$ , $\text{SO}_2$ Concentrations by Using Passive Samplers

The concentrations of the precursor gases ( $\text{NH}_3$ ,  $\text{NO}_2$ ,  $\text{SO}_2$ ),  $C_p$  (ppb), using the passive samplers were calculated using Equation 2.9:

$$C_p \text{ (ppb)} = \alpha_g * \frac{m_g}{t} \quad (2.9)$$

Where  $\alpha_g$  is the ppb concentration conversion coefficient (ppb – min/ng) for the precursor gas provided by RTI International,  $m_g$  is the mass loading on the pad (ng), and  $t$  is

passive sampling time (min). The duplicate samples were averaged and converted to  $\mu\text{g}/\text{m}^3$  using Equation 2.10:

$$C_p (\mu\text{g}/\text{m}^3) = \frac{P}{R * T} * ppm * MW * 10^3 \quad (2.10)$$

Where P is the atmospheric pressure (1 atm), R is the universal gas constant (0.082 L\*atm/mol\*K), T the average temperature of the sampling event (K), MW is the molecular weight of the gas of interest, and ppm is the volume concentration of the precursor gas of interest (1ppm = 1000 ppb in equation 2.9).

Since  $\text{H}_2\text{SO}_4$  is highly reactive and almost never exists in the gas-phase, its precursor gas,  $\text{SO}_2$ , was captured and stoichiometrically converted into  $\text{H}_2\text{SO}_4$ .  $\text{SO}_2$  is also highly reactive, so measured values were assumed to 100% convert to  $\text{H}_2\text{SO}_4$ . Using the reaction from equation 1.8, the conversion of  $\text{SO}_2$  to  $\text{H}_2\text{SO}_4$  was calculated using Equation 2.11:

$$C_{\text{H}_2\text{SO}_4} = \frac{C_{\text{SO}_2}}{MW_{\text{SO}_2}} * MW_{\text{H}_2\text{SO}_4} \quad (2.11)$$

Where  $C_{\text{H}_2\text{SO}_4}$  is the concentration of  $\text{H}_2\text{SO}_4$  ( $\mu\text{g}/\text{m}^3$ ),  $C_{\text{SO}_2}$  is the concentration of  $\text{SO}_2$  ( $\mu\text{g}/\text{m}^3$ ),  $MW_{\text{SO}_2}$  is the molecular weight of  $\text{SO}_2$  (64.066 g/mol), and  $MW_{\text{H}_2\text{SO}_4}$  is the molecular weight of  $\text{H}_2\text{SO}_4$  (98.079 g/mol).

#### **2.5.4 $\text{NO}_2$ Conversion**

An important input parameter for the ISORROPIA-II model is the concentration of  $\text{HNO}_3$ .  $\text{HNO}_3$  was converted from  $\text{NO}_2$ , which was assumed to follow the reaction shown in equation 1.9. However, since the reaction was mainly dictated by sunlight, not all  $\text{NO}_2$  might convert into  $\text{HNO}_3$ . Based on the reaction in Equation (1.6),  $\text{NO}_2$  was stoichiometrically

converted to HNO<sub>3</sub> using NO<sub>2</sub> molar ratio from the output of a 2016 simulation from the CMAQ model shown in Equation 2.12:

$$[HNO_3] = \frac{(1-\alpha)*[NO_2]}{\alpha} \quad (2.12)$$

Where [NO<sub>2</sub>] is the molar concentration of NO<sub>2</sub> in mol/m<sup>3</sup>, [HNO<sub>3</sub>] is the molar concentration of HNO<sub>3</sub> in mol/m<sup>3</sup>, and α is the molar ratio of NO<sub>2</sub>-HNO<sub>3</sub> from the CMAQ model. The molar ratios of NO<sub>2</sub>-HNO<sub>3</sub> for each sampling day from the most up to date CMAQ simulation is shown in Table 2.4.

**Table 2.4. NO<sub>2</sub> molar ratios**

Date	NO <sub>2</sub> -HNO <sub>3</sub> molar ratio	Date	NO <sub>2</sub> -HNO <sub>3</sub> molar ratio
11 Jul 2016	0.730192	25 Oct 2016	0.829707
12 Jul 2016	0.740376	26 Oct 2016	0.868615
12 Aug 2016	0.899162	27 Oct 2016	0.943283
13 Aug 2016	0.870936	16 Nov 2016	0.834558
14 Aug 2016	0.881993	17 Nov 2016	0.831486
17 Aug 2016	0.863666	18 Nov 2016	0.901784
18 Aug 2016	0.854005	10 Dec 2016	0.885833
23 Aug 2016	0.77999	11 Dec 2016	0.929169
24 Aug 2016	0.764735	12 Dec 2016	0.977064
25 Aug 2016	0.74912	13 Dec 2016	0.975382

## **2.6 Atmospheric Chemical Condition Analysis**

The concentrations of NH<sub>3</sub> from the denuders, passive samplers' H<sub>2</sub>SO<sub>4</sub> and HNO<sub>3</sub>, and NH<sub>4</sub><sup>+</sup>, SO<sub>4</sub><sup>-2</sup>, and NO<sub>3</sub><sup>-</sup> on the nylon filter were used to calculate the atmospheric chemical conditions shown in equations 1.10-1.15. Each atmospheric chemical condition was then plotted on a pollution rose graph using wind direction data from the local weather station. Each chemical condition was divided by station and season for analysis.

## 2.7 PM<sub>2.5</sub> MASS CLOSURE ANALYSIS

The contribution of iPM<sub>2.5</sub> to total PM<sub>2.5</sub> mass was analyzed using a mass closure profile of all of the PM<sub>2.5</sub> components. The profile includes the inorganic ions such as NH<sub>4</sub><sup>+</sup>, Na<sup>+</sup>, Cl<sup>-</sup>, SO<sub>4</sub><sup>-2</sup>, HSO<sub>4</sub><sup>-2</sup>, NO<sub>3</sub><sup>-</sup>, up to 33 elements, EC, and OC. A percent composition of each PM<sub>2.5</sub> component was found by dividing the concentration of each PM<sub>2.5</sub> component by the PM<sub>2.5</sub> concentration measured on the Teflon filter, which represented the total mass of PM<sub>2.5</sub>.

## 2.8 ISOROPPIA-II MODELING

The ISORROPIA-II model was used to simulate the gas-particle partitioning of NH<sub>3</sub>-NH<sub>4</sub><sup>+</sup>. The thermodynamic stable state and metastable state were applied for all simulations and the performances of both states were compared. The forward mode was applied in all simulations, where field measured data such as temperature, RH, total NH<sub>3</sub>, aerosol H<sub>2</sub>SO<sub>4</sub>, total HNO<sub>3</sub>, and concentrations of Na, Cl, Ca, K, and Mg were used as inputs. A sensitivity analysis was also conducted to analyze the responses of PM<sub>2.5</sub> to changes in precursor gases and temperature/RH.

## 2.9 STATISTICAL ANALYSIS

Data was analyzed with R programming software (version 4.2.2). The mean differences for each chemical parameter at each station during each season were tested using analysis of variance (ANOVA). Both season and station were considered two independent factors for the ANOVA test and the interactions were considered significant at  $p < 0.05$ . Tukey HSD test was used to check differences among sample means for significance. Trend line with 95% confidence intervals were graphed using ggplot2 package in R.

## CHAPTER 3: RESULTS AND DISCUSSION

### 3.1 COMPARISON OF PASSIVE SAMPLERS AND DENUDERS FOR NH<sub>3</sub> MEASUREMENTS

Comparison of the Ogawa passive samplers and honeycomb denuders for NH<sub>3</sub> sampling is shown in Figure 3.1. Both sampling methods have similar trends where NH<sub>3</sub> concentrations were higher in the summer and lower in the winter, which agrees with the findings of Walker et al., (2006), and Li et al., (2013). The time weighted averages from the passive sampler were higher than the 24 hr concentrations of the denuder samples.

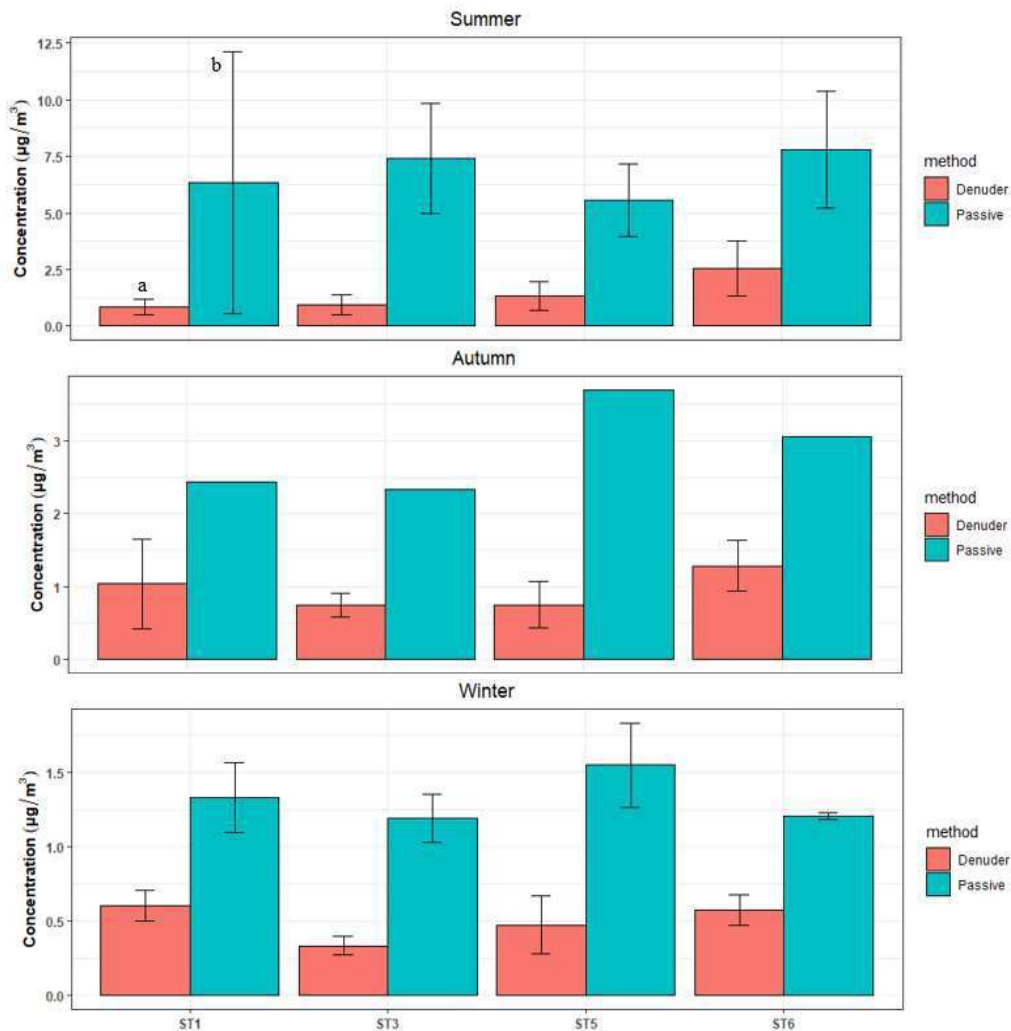


Figure 3.1. Boxplots of NH<sub>3</sub> concentrations measured by honeycomb denuder & passive samplers

The summary statistics of the denuder measurements are shown in Table 3.1. When comparing the NH<sub>3</sub> concentrations reported by Walker et al., (2006), and Li et al., (2013), the ambient concentrations at this research site were low which was due to the low bird population ranging between 1366 to 1355 throughout this study. There were significant differences in mean concentrations among different stations and over different seasons. The variation in the 24 hr denuder measurements could be an indication of an outside factor such as wind. It is also important to note that the exhaust from house 7 was facing towards the east. Based on this variation in the 24 hr data, the NH<sub>3</sub> passive sampler data was not used for any of the analysis conducted since the sampling duration of the passive samplers ranged between 1 to 2 weeks.

**Table 3.1. NH<sub>3</sub> concentrations measured through sampling by Denuders**

Season	Location	NH <sub>3</sub> (µg/m <sup>3</sup> )
Summer	ST1	0.843 ± 0.359 <sup>b</sup>
	ST3	0.953 ± 0.442 <sup>b</sup>
	ST5	1.341 ± 0.623 <sup>b</sup>
	ST6	2.554 ± 1.22 <sup>a</sup>
Autumn	ST1	1.038 ± 0.615
	ST3	0.743 ± 0.160
	ST5	0.753 ± 0.314
	ST6	1.2861 ± 0.351
Winter	ST1	0.603 ± 0.103 <sup>a</sup>
	ST3	0.336 ± 0.061 <sup>b</sup>
	ST5	0.476 ± 0.194 <sup>a,b</sup>
	ST6	0.575 ± 0.106 <sup>a</sup>

Passive sampling has its advantage of its low detection limit and small workload requirement, however, for modeling and chemical condition calculation investigation, the long sampling duration (days to weeks) from the passive sampler could not account for the changes in wind direction throughout each sampling event, so calculations could lead to misleading and incorrect results. On the other hand, the honeycomb denuder also has a low detection limit of < 0.01 µg/m<sup>3</sup> for NH<sub>3</sub> capture in 24 hrs (Sutton et al., 2001), which is applicable to this study since the ambient NH<sub>3</sub> concentrations was low in this environment.

The mean  $\pm$  SD of NO<sub>2</sub> and SO<sub>2</sub> measured by the Ogawa passive sampler was summarized in Table 3.2. The measured SO<sub>2</sub> was low as expected with lower concentrations in the summer and higher in the winter. For NO<sub>2</sub>, concentrations were higher than expected with lower concentrations in the summer and higher in the winter.

**Table 3.2. NO<sub>2</sub> and SO<sub>2</sub> concentrations measured by Ogawa passive sampler**

Season	Location	NO <sub>2</sub> (µg/m <sup>3</sup> )	SO <sub>2</sub> (µg/m <sup>3</sup> )
Summer	ST1	4.254 $\pm$ 1.298	0.117 $\pm$ 0.198
	ST2	3.388 $\pm$ 0.515	0.000
	ST5	2.662 $\pm$ 0.298	0.141 $\pm$ 0.298
	ST6	3.739 $\pm$ 0.541	0.183 $\pm$ 0.550
Autumn	ST1	5.485	0.179
	ST2	4.633	0.000
	ST5	3.997	0.000
	ST6	0.341	0.342
Winter	ST1	7.667 $\pm$ 0.850	0.417 $\pm$ 0.326
	ST2	6.774 $\pm$ 0.861	0.456 $\pm$ 0.323
	ST5	5.776 $\pm$ 1.91	0.598 $\pm$ 0.457
	ST6	7.031 $\pm$ 0.968	0.242 $\pm$ 0.099

### 3.2 ATMOSPHERIC CHEMICAL CONDITIONS

The means of the five chemical condition metrics defined by equations 1.10 – 1.15 for three seasons at different sampling stations are summarized in Table 3.3. As indicated by GR values, at all four stations, there was sufficient NH<sub>3</sub> to neutralize SO<sub>4</sub><sup>2-</sup> and NO<sub>3</sub><sup>-</sup> (GR > 1) for all three seasons. As for PNR values, particle neutralization potential was significantly higher in winter than in summer and autumn at all four sampling stations. Although ambient NH<sub>3</sub> was low in winter, high PNR values were observed due to low SO<sub>4</sub><sup>2-</sup> and NO<sub>3</sub><sup>-</sup> (Equation 1.12) from low concentrations of the precursor gases SO<sub>2</sub> and NO<sub>2</sub>. Moreover, extremely low SO<sub>2</sub> concentrations also led to the inability to calculate TA/TS (Equation 1.13). More sample collection is needed to truly understand dynamic changes of particle neutralization potential and TA/TS ratio in this rural environment. As for NH<sub>3</sub>/NH<sub>x</sub> results, greater than 0.5 at all stations and in all three seasons indicates that there was a greater amount of NH<sub>3</sub> in the gas phase than

NH<sub>4</sub><sup>+</sup> in the particle phase. This is more proof of insufficient precursor acid gases SO<sub>2</sub> and NO<sub>x</sub> to neutralize gas phase NH<sub>3</sub>. When examining the average AN/PM<sub>2.5</sub> ratio, it is observed that percentage of NH<sub>3</sub> sensitive PM<sub>2.5</sub> mass to total PM<sub>2.5</sub> mass was lower than 5% which is an indication that formation of secondary NH<sub>3</sub>-related PM<sub>2.5</sub> was low.

**Table 3.3 Mean ± SD of the chemical condition metrics separated by season and location**

Season	Location	Chemical Conditions				
		GR or AdjGR <sup>[1]</sup>	PNR	TA/TS	NH <sub>3</sub> /NH <sub>x</sub>	AN/PM <sub>2.5</sub>
Summer	ST1	2.624 ± 1.619 <sup>a, [2]</sup>	0.988 ± 1.651 <sup>a</sup>	28.590 ± NA <sup>[3]</sup>	0.984 ± 0.013	0.010 ± 0.011
	ST3	3.528 ± 1.973 <sup>b</sup>	0.591 ± 0.447 <sup>b</sup>	84.686 ± NA	0.981 ± 0.018	0.015 ± 0.015
	ST5	5.572 ± 1.886 <sup>b</sup>	1.062 ± 1.115 <sup>a,b</sup>	NA <sup>[4]</sup>	0.986 ± 0.110	0.008 ± 0.007
	ST6	9.683 ± 5.221 <sup>b</sup>	2.268 ± 1.088 <sup>a</sup>	NA	0.992 ± 0.006	0.004 ± 0.002
Autumn	ST1	3.314 ± 0.932	0.365 ± NA	18.256 ± NA	0.954 ± 0.021	0.018 ± 0.024
	ST3	3.205 ± 1.247	0.087 ± 0.021	9.323 ± NA	0.972 ± 0.025	0.018 ± 0.017
	ST5	3.653 ± 1.532	0.164 ± NA	8.239 ± NA	0.972 ± 0.021	0.013 ± 0.018
	ST6	5.771 ± 2.067	1.964 ± NA	NA	0.977 ± 0.009	0.007 ± 0.003
Winter	ST1	1.133 ± 0.360	5.765 ± 4.701	NA	0.798 ± 0.075 <sup>a</sup>	0.036 ± 0.031
	ST3	1.855 ± 1.299	0.859 ± NA	NA	0.971 ± 0.006 <sup>b</sup>	0.002 ± 0.002
	ST5	2.213 ± 1.928	3.112 ± 2.284	NA	0.858 ± 0.069 <sup>a,b</sup>	0.020 ± 0.016
	ST6	2.378 ± 1.076	4.013 ± 3.112	74.722 ± 29.017	0.754 ± 0.163 <sup>a</sup>	0.042 ± 0.041

<sup>[1]</sup>only winter season, data are in AdjGR; <sup>[2]</sup> means with different letters within a season indicate significant difference at  $p < 0.05$ ; <sup>[3]</sup> NA of SD indicates that TS was extremely low, only one TA/TS ratio was obtained such that no standard deviation was available; <sup>[4]</sup> NA of mean indicates that no TA/TS ratio was obtained for the sampling events due to unavailability of TS at the locations.

### 3.2.1 Spatial and Temporal Variations of GR & AdjGR as Impacted by Wind Direction

The spatial and temporal variations of AdjGR was plotted with wind direction on a pollution rose graph shown in Figure 3.2. During the summer, all stations had a AdjGR > 1 which is an indication of NH<sub>3</sub>-rich conditions. The pollution rose showed that ST1 was downwind from house 7 (the only house with birds during the study) and the manure shed while ST3 was downwind from the manure shed. The pollution rose also reveals that ST6 was geographically downwind from the manure shed with southeasterly winds, but more frequent

southerly winds affected GR the most. Google Maps indicated that approximate distances from the shed to ST1, ST3, and ST6 were 0.9 km, 0.5 km, and 0.4 km, respectively. Station 1 was the furthest from the manure shed, 0.9 km, and had only one instance where there was enough  $\text{NH}_3$  to only neutralize  $\text{SO}_4^{-2}$  ( $0 < \text{GR} < 1$ ).

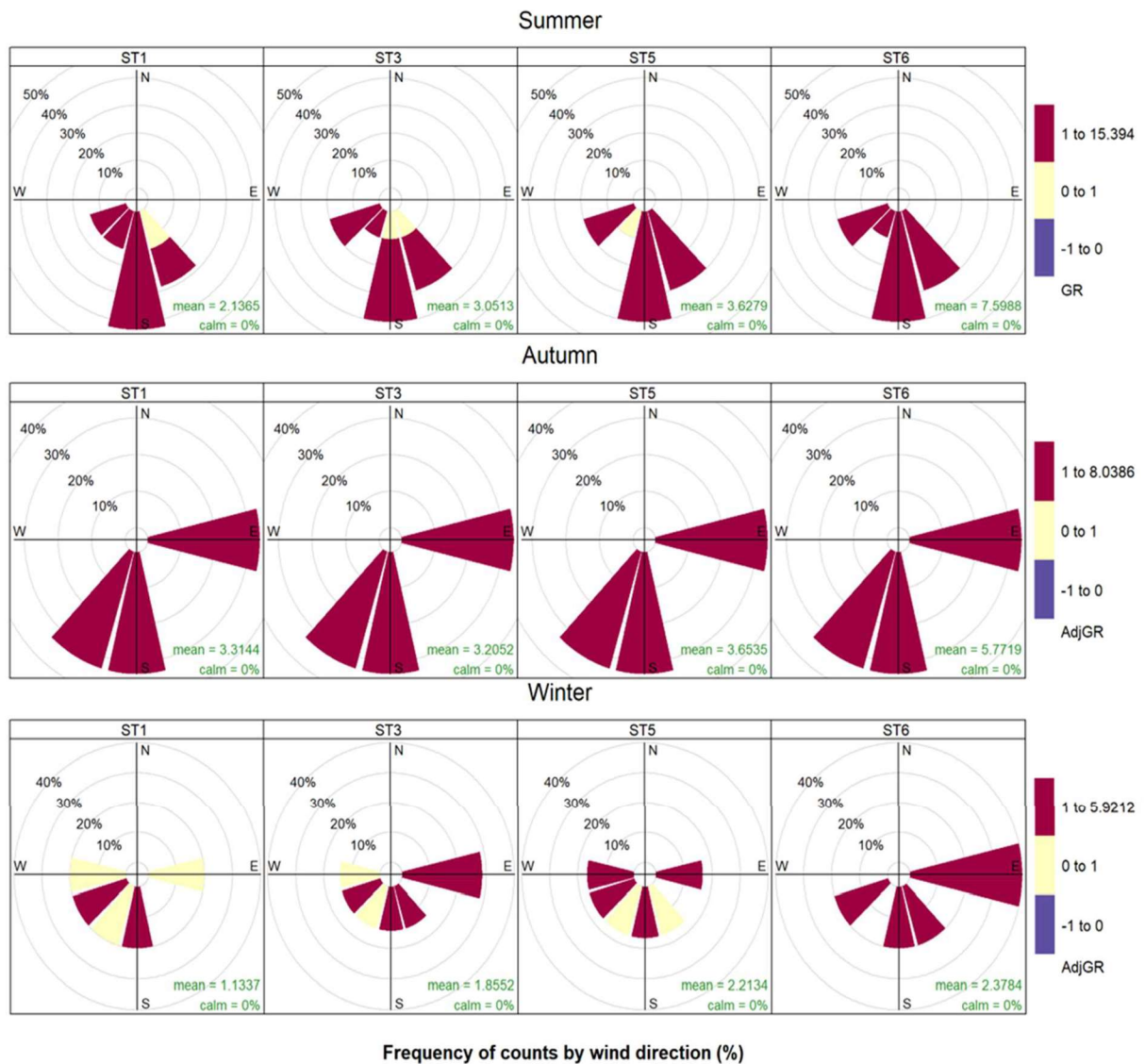


**Figure 3.2.** The AdjGR due to changes in wind direction separated by sampling station and season

In the autumn, there were  $\text{NH}_3$ -rich conditions at all stations with southerly, southwesterly, and easterly wind directions. Based on Figure 3.2, all of the stations were

downwind from a source during the autumn sampling period. With easterly winds, ST6 was downwind from house 7 while ST5 was downwind from the manure shed shown in figure 2.2. With southerly winds, ST1 became the downwind station from house 7 and the manure shed while ST3 was only downwind from the manure shed.

During the winter, the wind direction varied between westerly, southwesterly, southerly, and easterly. All stations, except for ST6, had instances of  $\text{NH}_3$ -rich conditions or enough  $\text{NH}_3$  to neutralize  $\text{SO}_4^{-2}$  only, which was due to a smaller sample size. Based on the observations of Figure 3.2 during the autumn, ST6 and ST5 were in a location favorable to becoming downwind with easterly winds. A study conducted by Cheng et al., (2021) also analyzed the spatial variation of GR in the southeast and discovered that an agricultural site and rural site downwind from AFO  $\text{NH}_3$  emissions experienced  $\text{NH}_3$ -rich conditions. Both sites were dominated by  $\text{NH}_3$ -poor conditions, but when the site was downwind and  $\text{GR} > 1$ , there was no  $\text{NH}_4^+$  formation due to low availability of acidic gases.

### ***3.2.2 Spatial and temporal variations of PNR as Impacted by Wind Direction***

The spatial and temporal variations in PNR for each station during each season are shown in Figure 3.3. During the summer season, there were instances where  $\text{PNR} > 1$  indicating that  $\text{NH}_3$ -related  $\text{iPM}_{2.5}$  was formed with southwesterly winds. There was only 1 instance where  $\text{PNR} > 1$  at ST6 in the autumn with southerly winds. During the winter, ST1, ST5, and ST6 all had  $\text{PNR} > 1$  with winds ranging between the west, south, and east. The PNR was consistently the highest during this period which is due to lower temperatures favoring  $\text{NH}_4\text{NO}_3$  formation.

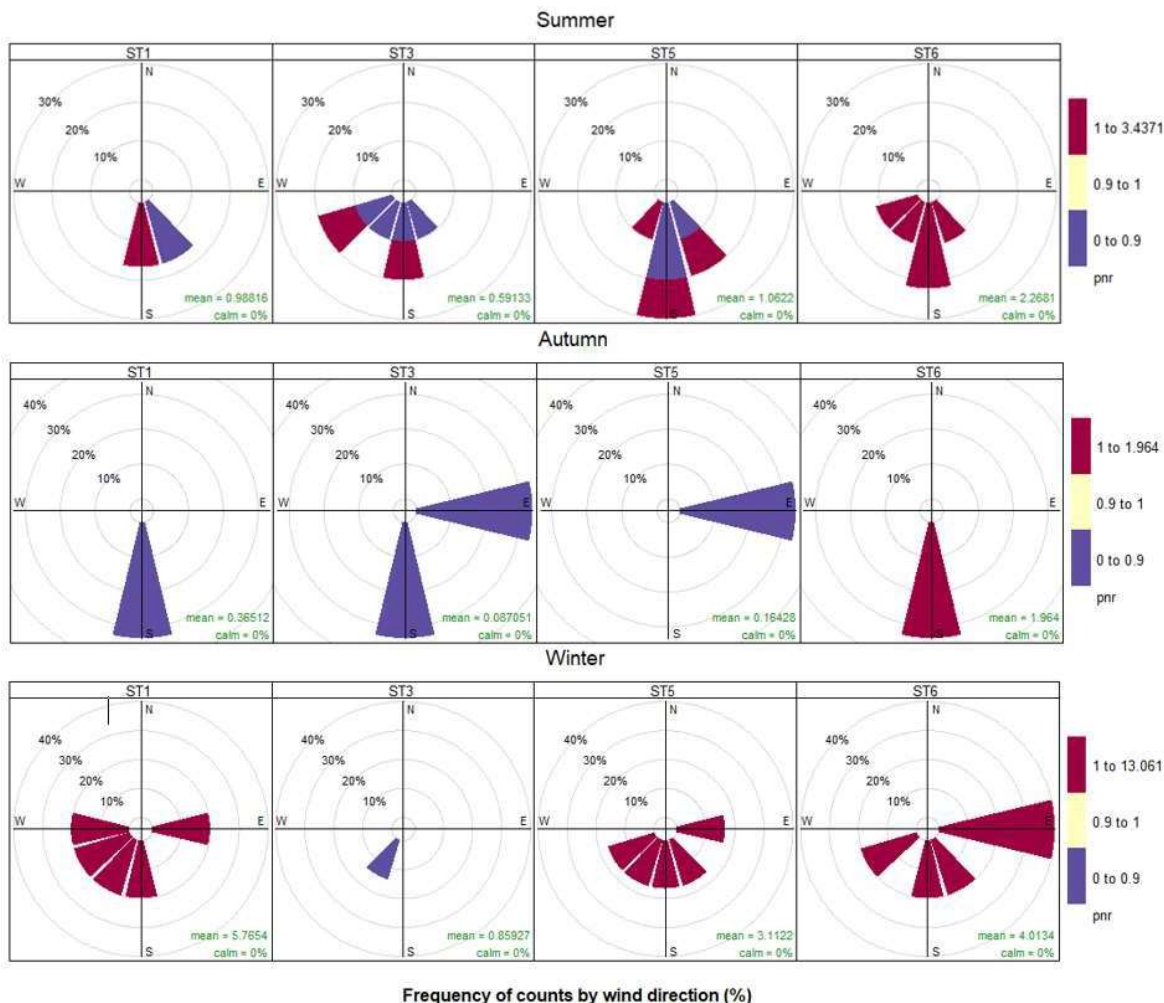


Figure 3.3. The PNR over changes of wind direction separated by sampling station and season

### 3.2.3 Spatial and temporal variations of $NH_3/NH_x$ as Impacted by Wind Direction

The spatial and temporal variations of  $NH_3/NH_x$  are shown in Figure 3.4. All stations during the summer and autumn showed that the  $NH_3/NH_x$  was closer to 1 with southern winds, which indicates that  $NH_3$  was predominantly in the gas phase. This agrees with the previous conditions with  $NH_3$  being rich in supply and a low PNR. During the winter,  $NH_3/NH_x$  was closer to 0.5 at ST1 and ST6 indicating that the conditions were closer to favoring equal amounts of  $NH_3$  in the gas phase and  $NH_4^+$  in the particle phase. This also agrees with the winter time AdjGR and PNR establishing rich  $NH_3$  conditions at all stations and  $iPM_{2.5}$  being saturated with

NH<sub>3</sub> at ST1, ST5, and ST6 indicating the formation of NH<sub>4</sub>NO<sub>3</sub>. The study conducted by Cheng et al., (2021) found NH<sub>3</sub>/NH<sub>x</sub> was higher when the agriculture site was downwind from AFOs due to the emitted NH<sub>3</sub>. The overall NH<sub>3</sub>/NH<sub>x</sub> had increased from 2004-2016 due to decreasing trends in SO<sub>2</sub> and NO<sub>2</sub>.

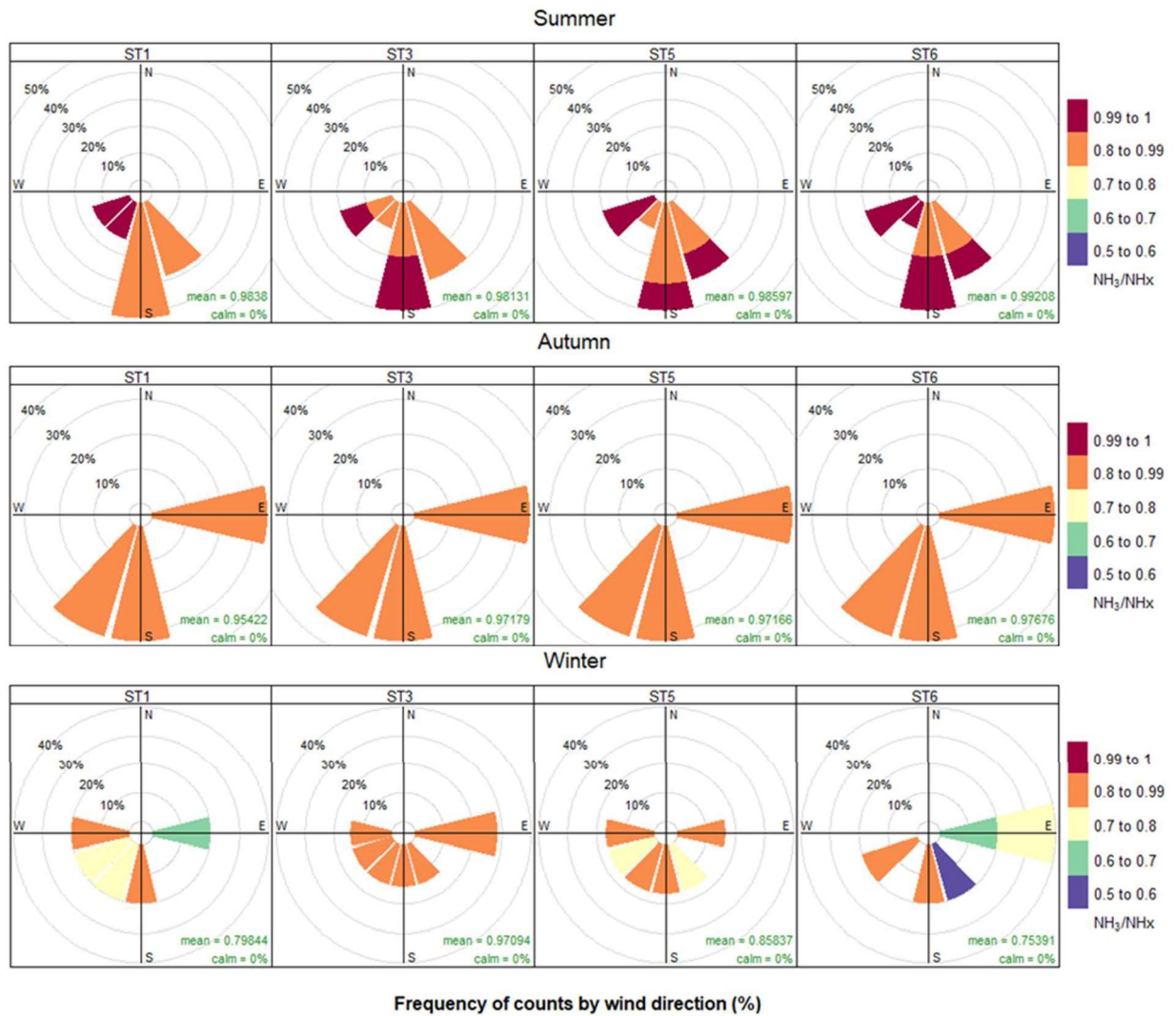


Figure 3.4. The NH<sub>3</sub>/NH<sub>x</sub> over changes of wind direction separated by sampling station and season

### 3.2.4 Spatial and temporal variations of TA/TS as Impacted by Wind Direction

The spatial and temporal variations of TA/TS are illustrated in Figure 3.5. According to Table 6, there were many values that could not be calculated due to the low concentrations of

SO<sub>4</sub><sup>-2</sup>. Whenever SO<sub>4</sub><sup>-2</sup> was available, TA/TS was always above 2 indicating that the conditions were less acidic and either (NH<sub>4</sub>)<sub>2</sub>SO<sub>4</sub> and NH<sub>4</sub>NO<sub>3</sub> may have existed in the particle phase. Of the calculated TA/TS, the observations agree with that found from Cheng et al., (2021) where TA/TS > 2. The two sites analyzed by Cheng et al., (2021) had overall increasing TA/TS due to decreasing SO<sub>2</sub> emissions between 2004-2016.

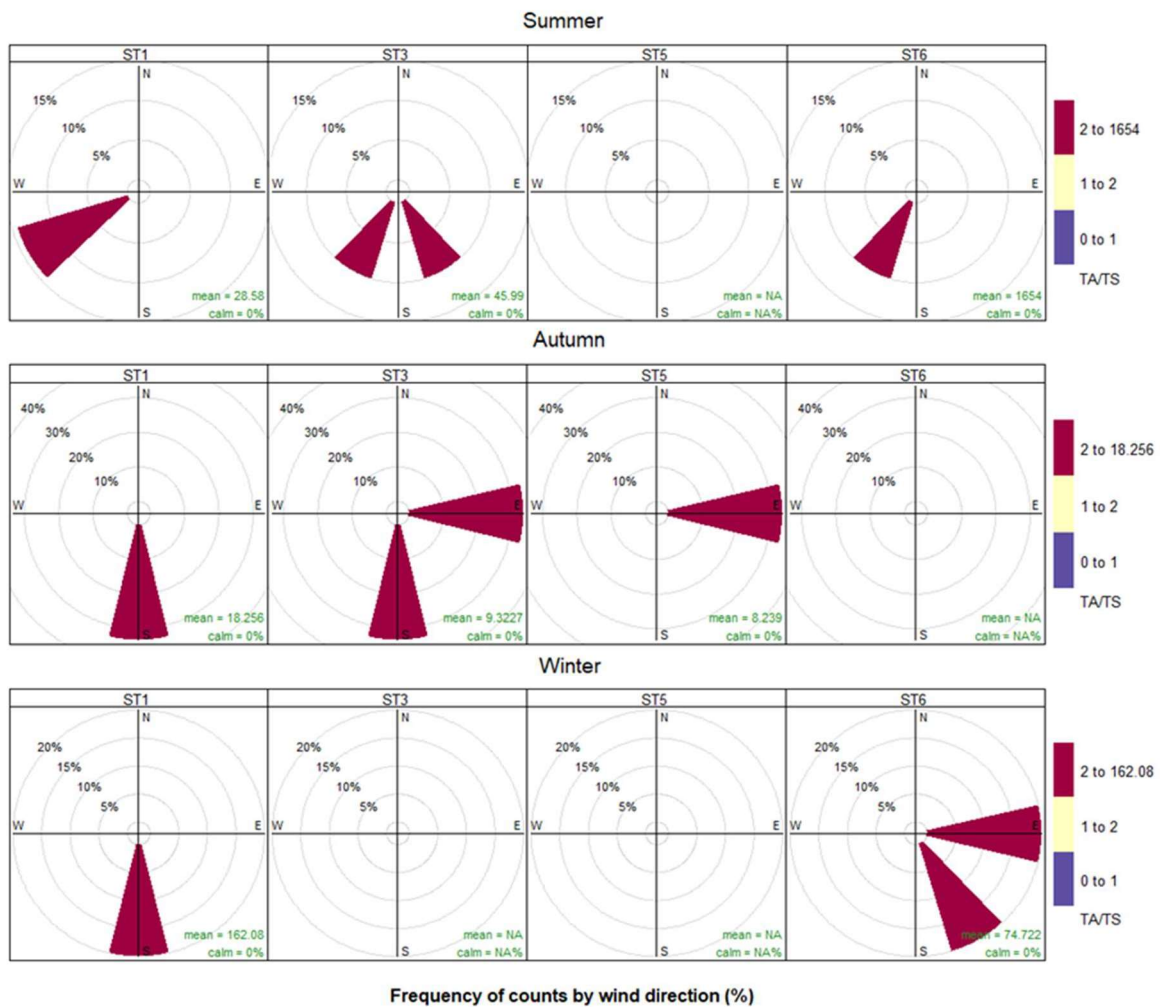


Figure 3.5. The TA/TS over changes of wind direction separated by sampling station and season

### 3.2.5 Spatial and temporal variations of AN/PM<sub>2.5</sub> as Impacted by Wind Direction

The spatial and temporal variations of AN/PM<sub>2.5</sub> are shown in Figure 3.6. During the summer, AN/PM<sub>2.5</sub> < 0.05 at ST1, ST3, ST5, and ST6 with southerly and southeasterly winds.

Based on the summer time PNR and  $\text{NH}_3/\text{NH}_x$  in Figure 3.3-3.4, there was  $\text{NH}_3$ -related  $\text{iPM}_{2.5}$  formed at all four stations, but  $\text{AN}/\text{PM}_{2.5} < 0.05$  indicates that this was a small amount. Since there were only 4 cases of TA/TS due to low  $\text{SO}_4^{2-}$ , the small amount of  $\text{iPM}_{2.5}$  formed was  $\text{NH}_4\text{NO}_3$ . The autumn season exhibited low  $\text{PM}_{2.5}$  fractions at all stations. During the winter, ST1 and ST6 had the highest cases where  $\text{AN}/\text{PM}_{2.5}$  was around 10%. Despite  $\text{AdjGR} > 1$ ,  $\text{PNR} > 1$ , and  $\text{NH}_3/\text{NH}_x$  approaching 0.5 in more frequent cases,  $\text{AN}/\text{PM}_{2.5}$  was still low which is an indication that the  $\text{PM}_{2.5}$  in this location is mainly consisted of organic content. Cheng et al., (2021) also found low  $\text{AN}/\text{PM}_{2.5}$  around 10% with the ratio being higher in the colder seasons and lower in warmer seasons.

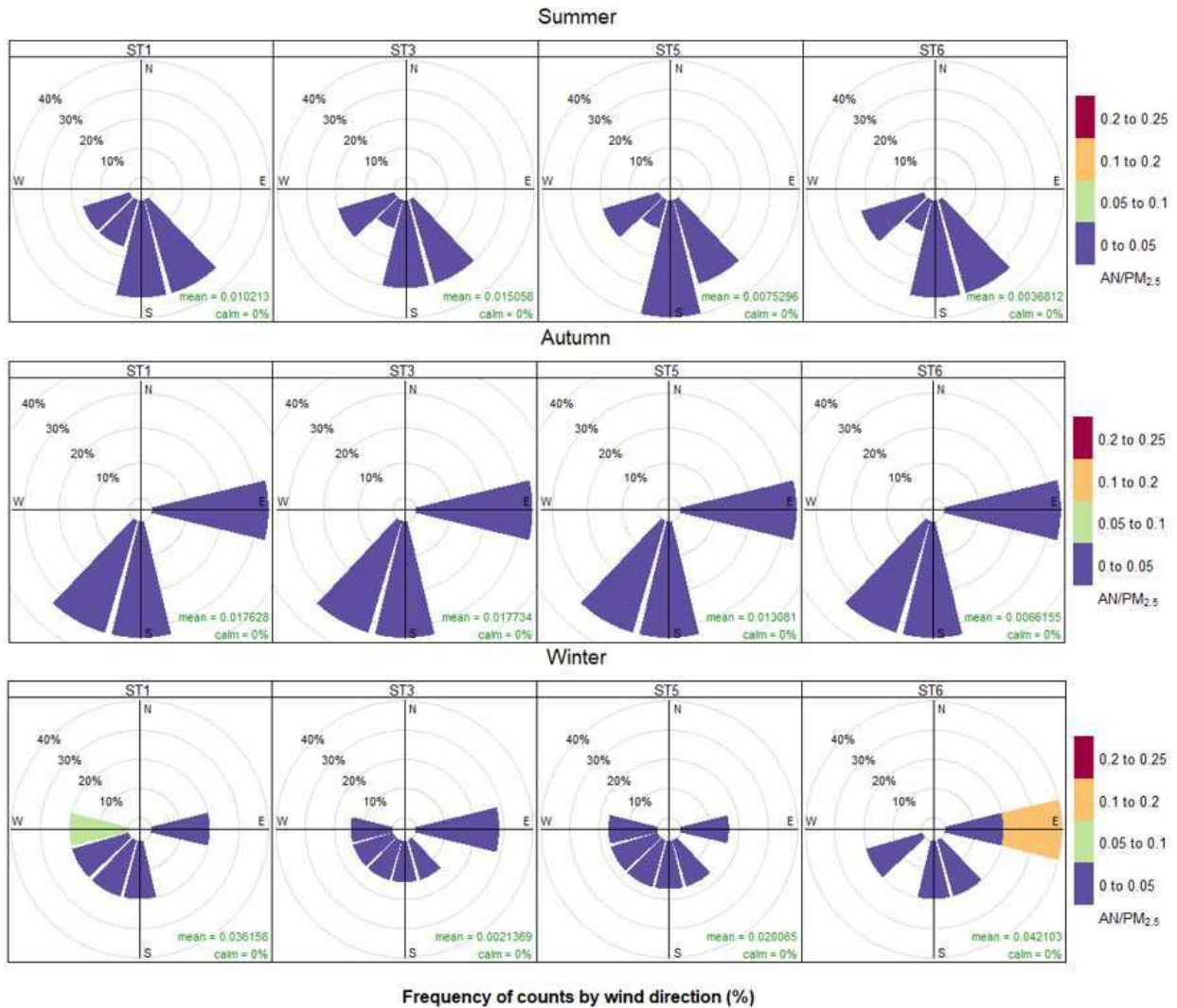


Figure 3.5. The AN/PM<sub>2.5</sub> over changes of wind direction separated by sampling station and season

### 3.3 PM<sub>2.5</sub> MASS CLOSURE

The PM<sub>2.5</sub> mass closure was initially calculated by dividing the sum of the measured chemical components of PM<sub>2.5</sub> by the total PM<sub>2.5</sub> concentration measured on the Teflon filter for each station during each season. However, there were 41 instances across all seasons and stations where the sum of PM<sub>2.5</sub> components were greater than the concentration measured on the Teflon filter. This was possibly due to uncertainty in filter handling and conditioning; therefore, PM<sub>2.5</sub> mass measured on Teflon filter was not used for analysis. Due to the large number of

disregarded sampling events in the previous analysis, the mass closure of the sum of PM<sub>2.5</sub> components was further analyzed. The mean ± SD was calculated for each species at each station during each season to be graphed for mass closure analysis. The mean ± SD values are shown in Table 3.4.

**Table 3.4. Mean ± SD for PM<sub>2.5</sub> and its Components in µg/m<sup>3</sup>**

Season	Location	Species							
		PM <sub>2.5</sub>	OC	EC	SO <sub>4</sub> <sup>-2</sup>	NO <sub>3</sub> <sup>-</sup>	NH <sub>4</sub> <sup>+</sup>	Elements	Inorganics**
Summer	ST1	6.58 ± 1.55 <sup>ab</sup>	5.25 ± 1.88	0.00	0.03 ± 0.09	0.52 ± 1.12	0.01 ± 0.01	0.42 ± 0.14	0.18 ± 0.18
	ST3	6.14 ± 1.97 <sup>a</sup>	6.45 ± 2.31	0.00	0.03 ± 0.07	0.44 ± 0.66	0.01 ± 0.01	0.39 ± 0.17	0.14 ± 0.08
	ST5	9.77 ± 4.25 <sup>b</sup>	5.90 ± 1.67	0.00	0.00	0.91 ± 1.02	0.02 ± 0.02	0.50 ± 0.16	0.12 ± 0.05
	ST6	8.23 ± 1.42 <sup>ab</sup>	6.45 ± 1.03	0.00	0.00	0.12 ± 0.17	0.01 ± 0.01	0.43 ± 0.09	0.08 ± 0.02
Autumn	ST1	7.84 ± 2.44	8.25 ± 2.98	0.44 ± 0.28	0.16 ± 0.21	0.13 ± 1.09	0.05 ± 0.04	0.43 ± 0.14	0.12 ± 0.07
	ST3	6.51 ± 2.22	9.63 ± 3.35	0.55 ± 0.28	0.61 ± 0.51	0.12 ± 0.65	0.02 ± 0.01	0.37 ± 0.18	0.09 ± 0.04
	ST5	7.33 ± 4.14	8.87 ± 3.89	0.47 ± 0.42	0.12 ± 0.21	0.05 ± 0.08	0.02 ± 0.01	0.35 ± 0.14	0.06 ± 0.03
	ST6	7.04 ± 3.86	8.23 ± 4.48	0.43 ± 0.43	0.00	0.02 ± 0.04	0.03 ± 0.01	0.43 ± 0.29	0.08 ± 0.03
Winter	ST1	7.70 ± 2.50	7.10 ± 2.93	0.14 ± 0.28	0.00 ± 0.20	0.10 ± 1.11 <sup>ab</sup>	0.12 ± 0.04 <sup>ab</sup>	0.46 ± 0.10	0.10 ± 0.01
	ST3	7.57 ± 2.31	8.13 ± 3.40	0.09 ± 0.28	0.000 ± 0.51	0.01 ± 0.671 <sup>a</sup>	0.01 ± 0.01 <sup>a</sup>	0.46 ± 0.18	0.06 ± 0.04
	ST5	7.53 ± 1.89	6.56 ± 2.27	0.00	0.00	0.09 ± 0.11 <sup>ab</sup>	0.06 ± 0.04 <sup>ab</sup>	0.43 ± 0.07	0.19 ± 0.28
	ST6	8.59 ± 5.02	7.06 ± 1.88	0.15 ± 0.33	0.02 ± 0.03	0.14 ± 0.11 <sup>b</sup>	0.16 ± 0.13 <sup>b</sup>	0.40 ± 0.05	0.30 ± 0.29

\*Means with different letter indicate significant difference; \*\*inorganics include Na<sup>+</sup>, Ca<sup>2+</sup>, Cl<sup>-</sup>, Mg<sup>+2</sup>, and K

The composition of PM<sub>2.5</sub> consists of inorganics, OC, EC, and 28 different elements.

These elements include Ag, Al, As, Ba, Br, Cd, Ce, Co, Cr, Cs, Cu, Fe, In, Mn, Ni, P, Pb, Rb, S, Sb, Se, Si, Sn, Sr, Ti, V, Zn, and Zr. For the mass closure, OC, EC, and elements were grouped in their own respective fractions. For the inorganics, NH<sub>4</sub><sup>+</sup>, SO<sub>4</sub><sup>-2</sup>, and NO<sub>3</sub><sup>-</sup> were separated from Na<sup>+</sup>, Ca<sup>2+</sup>, Cl<sup>-</sup>, Mg<sup>+2</sup>, and K to evaluate the NH<sub>3</sub> contribution to iPM<sub>2.5</sub> fractions.

Figure 3.6-3.8 shows the PM<sub>2.5</sub> chemical speciation mass fractions in the summer, autumn, and winter, respectively. For all stations during each season, OC was the main component of PM<sub>2.5</sub> at this site ranging between 80% to 93% of the total PM<sub>2.5</sub> composition. A similar analysis conducted by Li et al., (2015) found the contribution of OC to be between 50%

to 55% of PM<sub>2.5</sub> composition at four different ambient stations on a commercial egg production farm in NC. Primary OC originates from biomass combustion and traffic while secondary OC forms from volatile organic compounds (VOCs) emissions from vegetation (Saarikoski et al., 2008; Jones & Harrison 2005; Wang et al., 2021). OC and EC have been found to contribute between 10%-80% of total PM<sub>2.5</sub> composition across different regions such as London, California, and China (Na et al., 2004; Harrison et al., 2004; Wang et al., 2015). Saarikoski et al., (2008) reported that 64% of OC was secondary in a European urban environment with high vegetation. In Figure 3.6, the fraction percentages of NH<sub>4</sub><sup>+</sup>, SO<sub>4</sub><sup>-2</sup>, and NO<sub>3</sub><sup>-</sup> were between 0% to 1% for all four stations. Based on the summer time GR and PNR in Figures 3.2-3.3, there was sufficient NH<sub>3</sub> for neutralization and NH<sub>3</sub>-related iPM<sub>2.5</sub> was formed. The iPM<sub>2.5</sub> fraction was small based on AN/PM<sub>2.5</sub> < 0.03. The 4 cases of TA/TS > 2 from the low SO<sub>4</sub><sup>-2</sup> presence indicate less acidic conditions and low contribution from H<sub>2</sub>SO<sub>4</sub>. This suggests that the iPM<sub>2.5</sub> formed was from NH<sub>3</sub> reacting with HNO<sub>3</sub>.

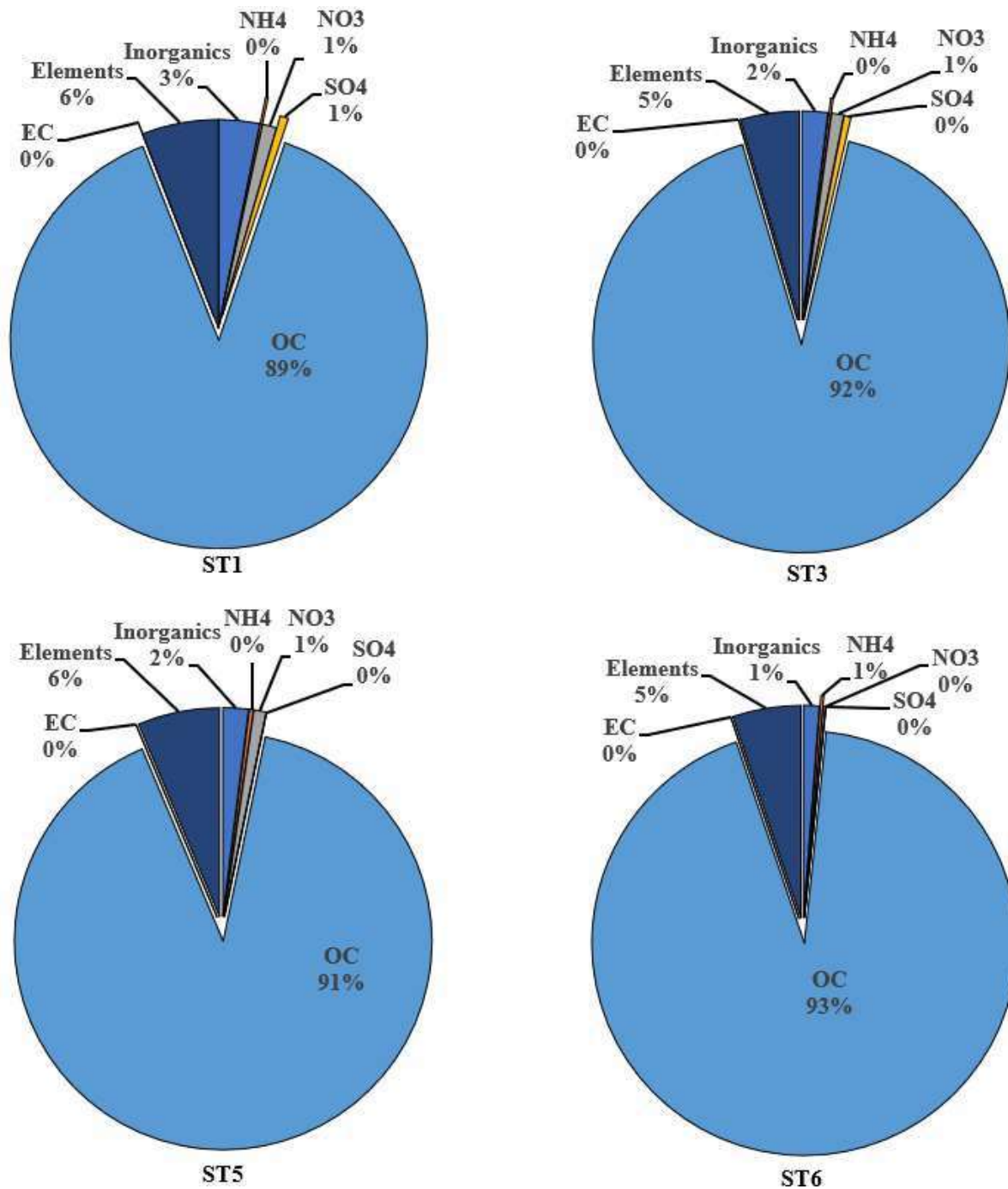


Figure 3.6. Summer PM<sub>2.5</sub> chemical speciation mass fractions; inorganics include Na<sup>+</sup>, Ca<sup>2+</sup>, Cl<sup>-</sup>, Mg<sup>2+</sup>, and K

In Figure 3.7, the fraction percentages of NH<sub>4</sub><sup>+</sup>, and NO<sub>3</sub><sup>-</sup> were between 0% to 2% for all four stations. Based on the atmospheric chemical parameters, there was a small formation of NH<sub>3</sub>-related iPM<sub>2.5</sub> similar to the summer. The EC fraction was at its highest, 5%, during the

autumn when compared to the other seasons. This can be attributed to biomass burning that was occurring on the research site during this period.

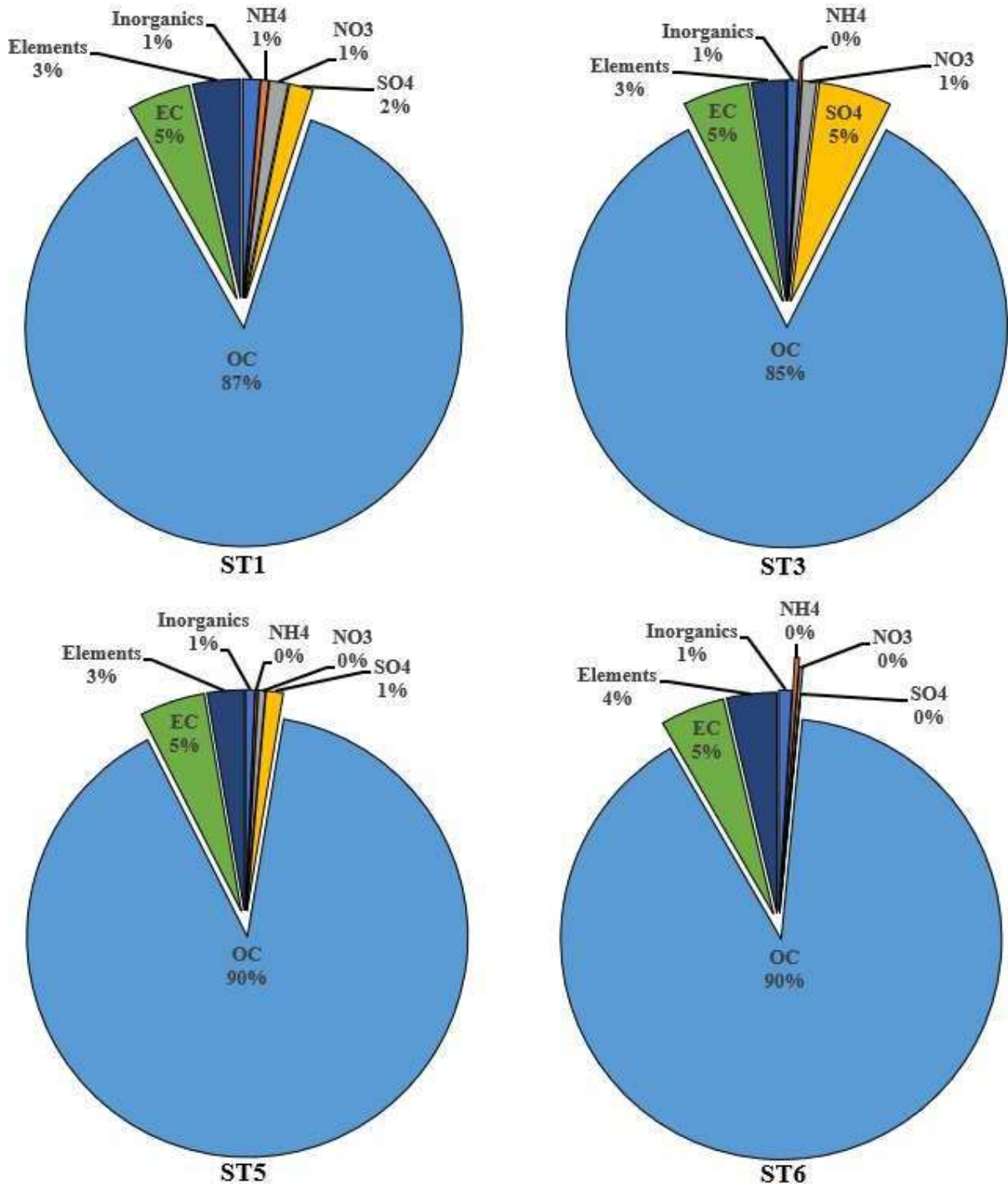


Figure 3.7. Autumn PM<sub>2.5</sub> chemical speciation mass fractions; inorganics include Na<sup>+</sup>, Ca<sup>2+</sup>, Cl<sup>-</sup>, Mg<sup>2+</sup>, and K

In Figure 3.8, the fraction percentages of  $\text{NH}_4^+$ , and  $\text{NO}_3^-$  were between 1% to 2% for ST1, ST5, and ST6. Based on the winter time GR and  $\text{NH}_3/\text{NH}_x$  in Figures 3.2 and 3.4, there were more cases where there was only enough  $\text{NH}_3$  to neutralize either  $\text{SO}_4^{2-}$  or  $\text{NO}_3^-$  and more particle-phase  $\text{NH}_4^+$  present. The PNR in Figure 3.3 indicates  $\text{NH}_3$ -related  $\text{iPM}_{2.5}$  formed, but the few cases of TA/TS indicates that  $\text{NO}_3^-$  was the dominant anion in  $\text{NH}_3$ -related  $\text{iPM}_{2.5}$ . Despite the  $\text{NH}_3$ -related  $\text{iPM}_{2.5}$  being the highest in the winter time based on Table 3.4, then highest AN/ $\text{PM}_{2.5}$  was only around 10% for the few cases shown in Figure 3.5, which was due OC being the dominant  $\text{PM}_{2.5}$  fraction at this site. A study conducted by Cheng et al., (2019) found that  $\text{NH}_4^+$  and  $\text{SO}_4^{2-}$  were higher in the summer and lower in the winter while  $\text{NO}_3^-$  was lower in the summer and higher in the winter at multiple investigated rural sites in the southeastern US. The OC fraction was also dominant in  $\text{PM}_{2.5}$  around 30% of the total composition for the rural sites and agricultural site during 2012-2016. A decrease in overall  $\text{NO}_2$  and  $\text{SO}_2$  concentrations in during the examined period increased OC/ $\text{PM}_{2.5}$  from 29.5% to 37.7% when Cheng et al., (2019) compared the 2001-2007 and 2012-2016 periods.

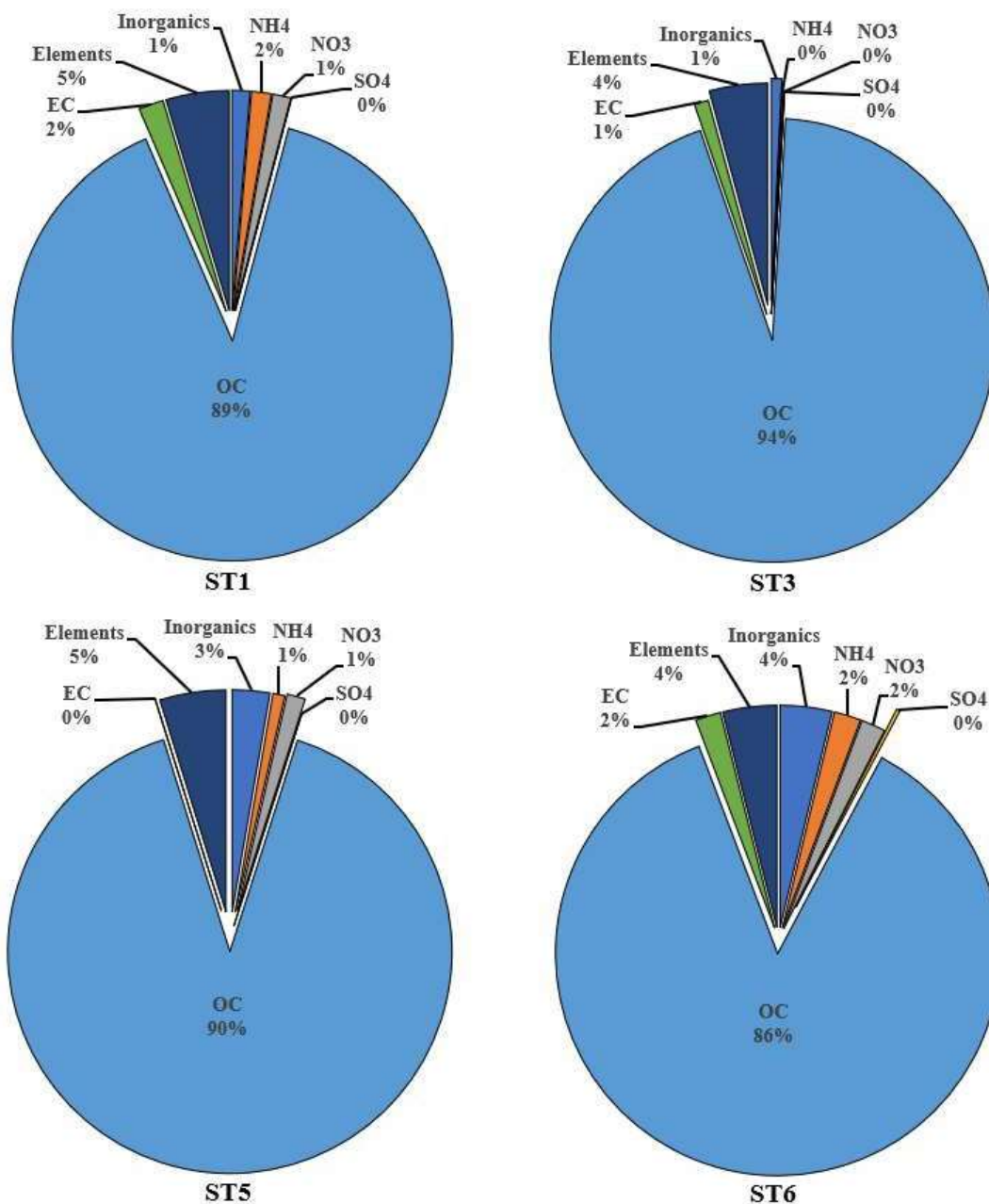


Figure 3.8. Winter PM<sub>2.5</sub> chemical speciation mass fractions; inorganics include Na<sup>+</sup>, Ca<sup>2+</sup>, Cl<sup>-</sup>, Mg<sup>2+</sup>, and K

### 3.4 ISOROPPIA-II MODELING

#### 3.4.1 Modeling with Passive Sampler HNO<sub>3</sub>

Measured values of NH<sub>3</sub>, NH<sub>4</sub><sup>+</sup>, SO<sub>4</sub><sup>-2</sup>, NO<sub>3</sub><sup>-</sup>, and Cl<sup>-</sup> from the PM<sub>2.5</sub> speciation samplers and measured HNO<sub>3</sub> from the passive sampler were compared to the modeled values, as shown

in Figure 3.9 and 3.10. Since all of  $\text{H}_2\text{SO}_4$  was assumed to react quickly and almost always existed in the particle phase, measurements of  $\text{SO}_4^{-2}$  from the nylon filters were only used for TS. Both the metastable and stable state of ISORROPIA-II were utilized for the simulations and showed little to no differences in the results. For  $\text{NH}_3$ , there was good agreement between the measured and simulated values with an  $R^2 = 0.94$ . However, there was poor agreement between measured and simulated  $\text{NH}_4^+$  as the model overpredicted 74% of the measured  $\text{NH}_4^+$  values. For  $\text{NO}_3^-$ , the model overpredicted 63% of measured values. As for  $\text{HNO}_3$ , the model predicted that over 50% of the measured values were in particle phase which could be a result of the low availability of  $\text{SO}_4^{-2}$ . The model predicted 56% of total  $\text{Cl}^-$  to partition in the gas phase, which could be due to the low concentrations of Cl. The results matched the concern raised by Cheng et al., (2022) where low time resolution data of  $\text{SO}_2$  and  $\text{NO}_2$  might not be able to detect variations of the gas-particle partitioning with changes in ambient conditions.

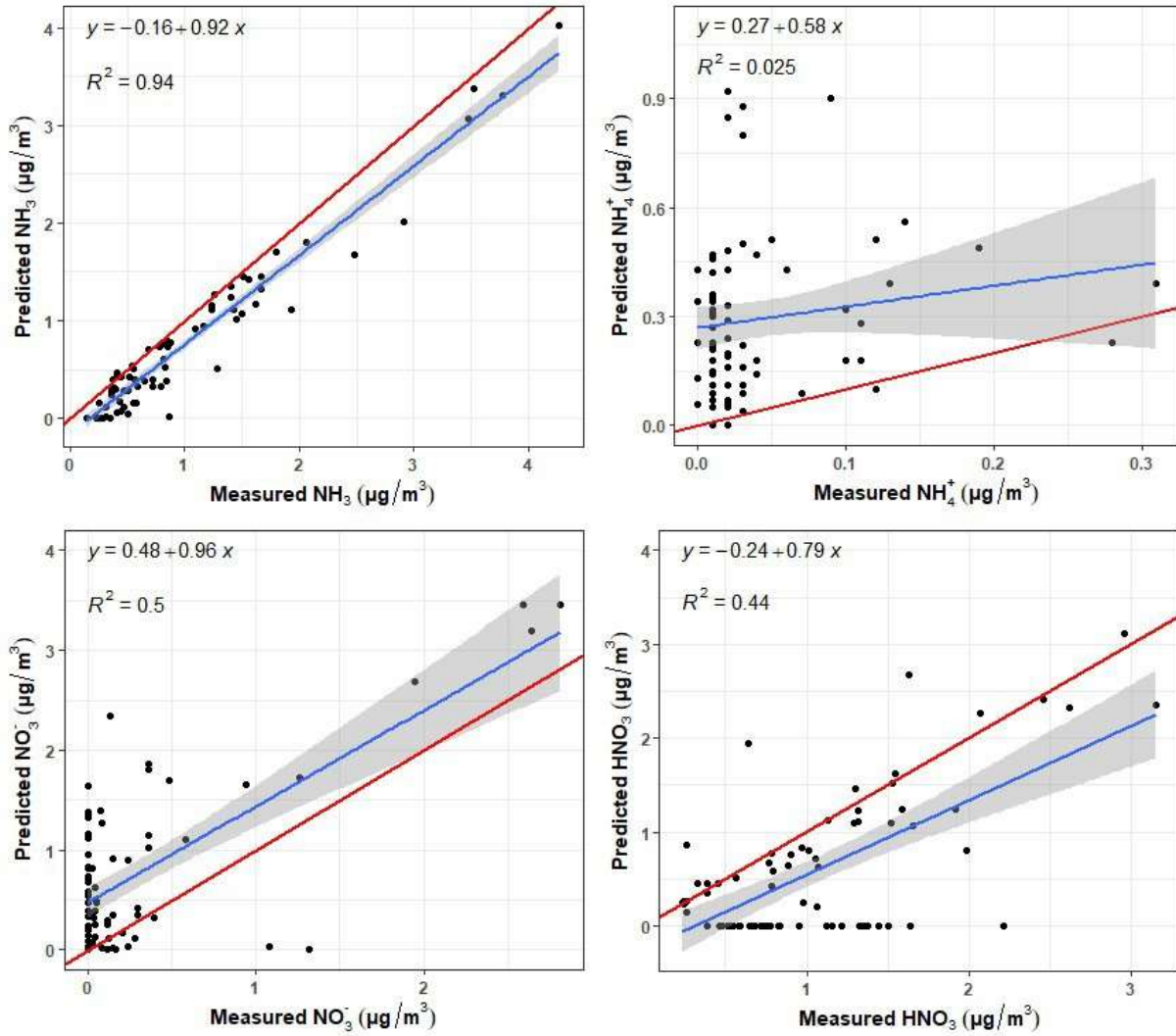
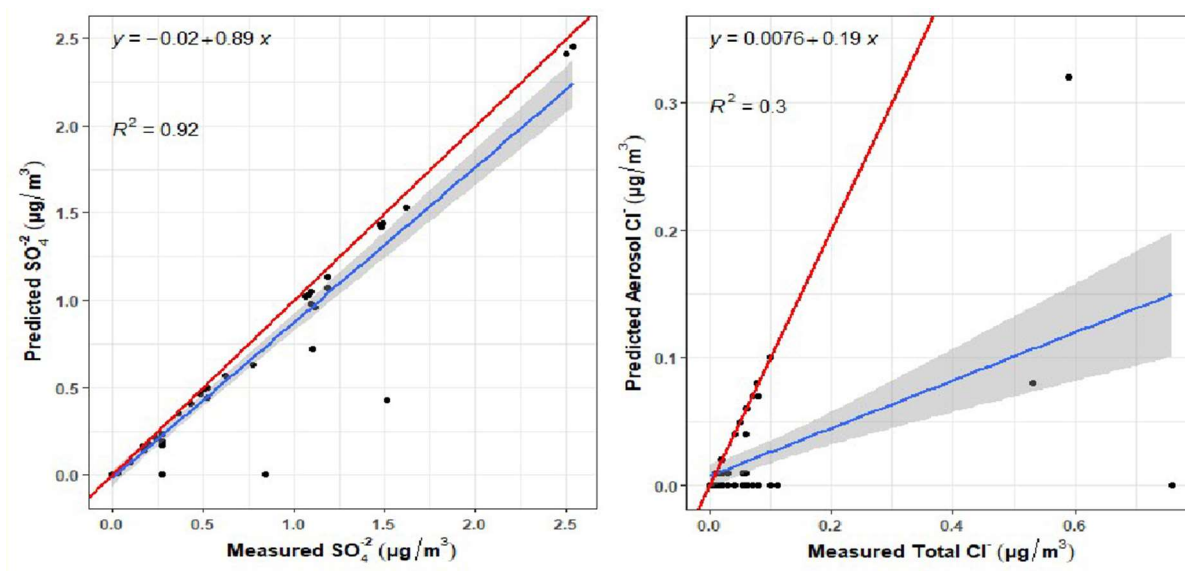


Figure 3.9. Comparison of ISORROPIA-II model results with passive sampler  $\text{HNO}_3$  with 1:1 slope line (red), regression line (blue), and 95% confidence interval (gray area)



**Figure 3.10. Comparison of ISORROPIA-II model results with passive sampler HNO<sub>3</sub> continued with 1:1 slope line (red), regression line (blue), and 95% confidence interval (gray area)**

### 3.4.2 Modeling with Chemical Speciation Data

Nylon filters have been reported to have a high collection efficiency for HNO<sub>3</sub> and HCl (Anlauf et al. 1985; Sturges and Harrison 1989; Masia et al. 1994; Mehlmann and Warneck 1995), when in series with a Teflon filter. Therefore, the nylon filter was assumed to still have a high collection efficiency. The data was first simulated using the metastable state and the predicted versus measured NH<sub>3</sub>, NH<sub>4</sub><sup>+</sup>, Total NO<sub>3</sub><sup>-</sup>, and SO<sub>4</sub><sup>-2</sup> are shown in Figure 3.11. For NH<sub>3</sub>, there was an improvement in model prediction as R<sup>2</sup> increased from 0.94 to 0.96. There was still poor agreement in predicting NH<sub>4</sub><sup>+</sup>, which might be a result of the high OC/PM<sub>2.5</sub> at the site. As previously reported by Silvern et al., (2017), NH<sub>4</sub><sup>+</sup>/SO<sub>4</sub><sup>-2</sup> was lower in the summer at a southeastern site which could be due to organic matter mixing with SO<sub>4</sub><sup>-2</sup> aerosols. Mixing these two aerosols may slow down NH<sub>3</sub> gas-particle partitioning by creating an organic film around the core of the particle (Anttila et al., 2007; Ciobanu et al., 2009; Bertram et al., 2011; Koop et

al., 2011; You et al., 2013). Liggio et al., (2011) also reported that  $\text{NH}_3$  neutralization was hindered by the presence of organic matter when it was tested in a laboratory. The model improved predicting  $\text{NO}_3^-$  indicated by  $R^2$  increasing from 0.5 to 0.88. The model perfectly predicted all measured  $\text{SO}_4^{2-}$ . The predicted  $\text{Cl}^-$  versus measured Total  $\text{Cl}^-$  is shown in Figure 3.12. There was a poor agreement between measured  $\text{Cl}^-$  and predicted  $\text{Cl}^-$  similar to the previous model results possibly due to low concentrations of total  $\text{Cl}^-$  since it was not a coastal site with a lack of  $\text{Cl}^-$  emission source. These results agree with observations found by Li et al., (2014a) and by Walker et al., (2006). There were similar results between the metastable and stable state; however, the model poorly predicted  $\text{SO}_4^{2-}$  as shown in Figure 3.13.

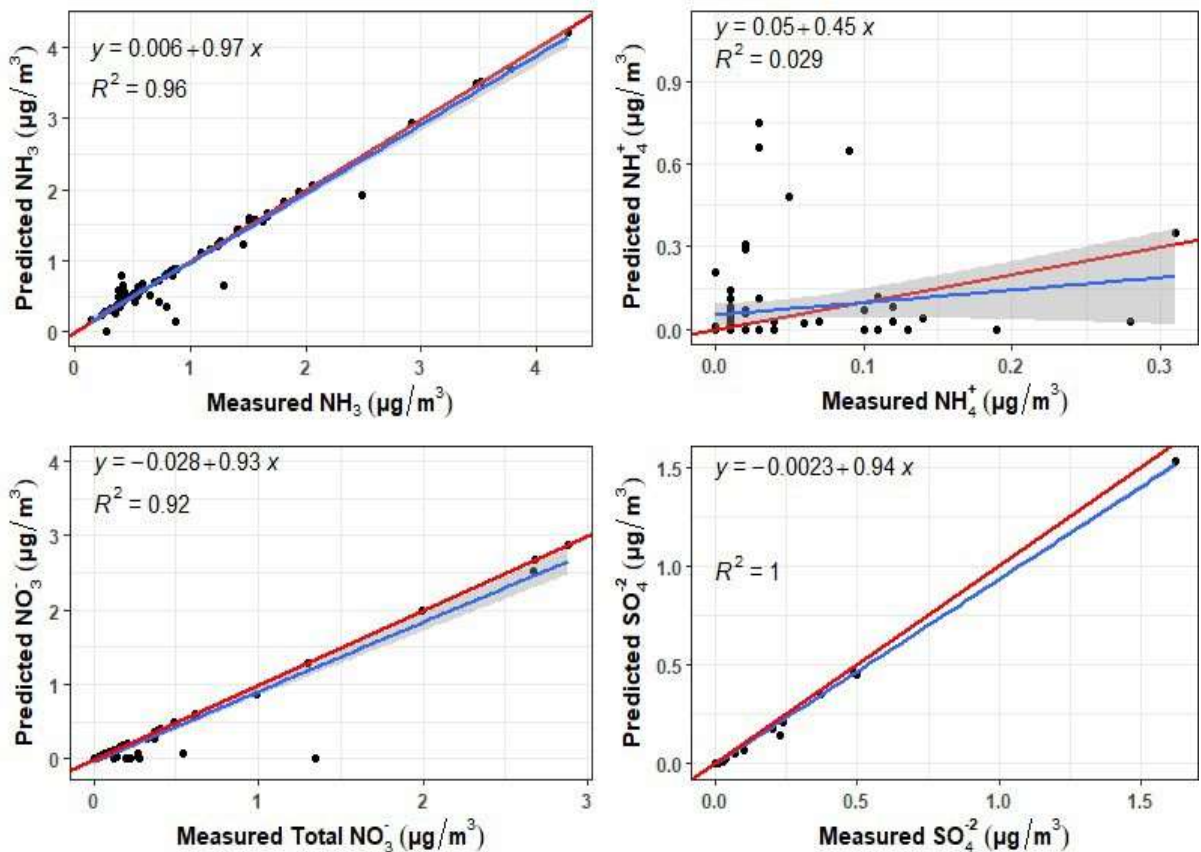


Figure 3.11. Comparison of ISORROPIA-II model results with speciation data measurements with 1:1 slope line (red), regression line (blue), and 95% confidence interval (gray area)

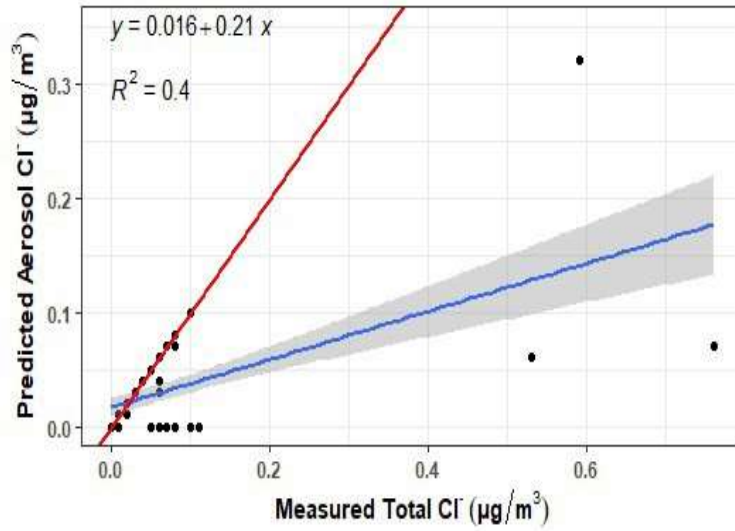


Figure 3.12. ISORROPIA-II predicted aerosol  $\text{Cl}^-$  vs. measured total  $\text{Cl}^-$  with 1:1 slope line (red), regression line (blue), and 95% confidence interval (gray area)

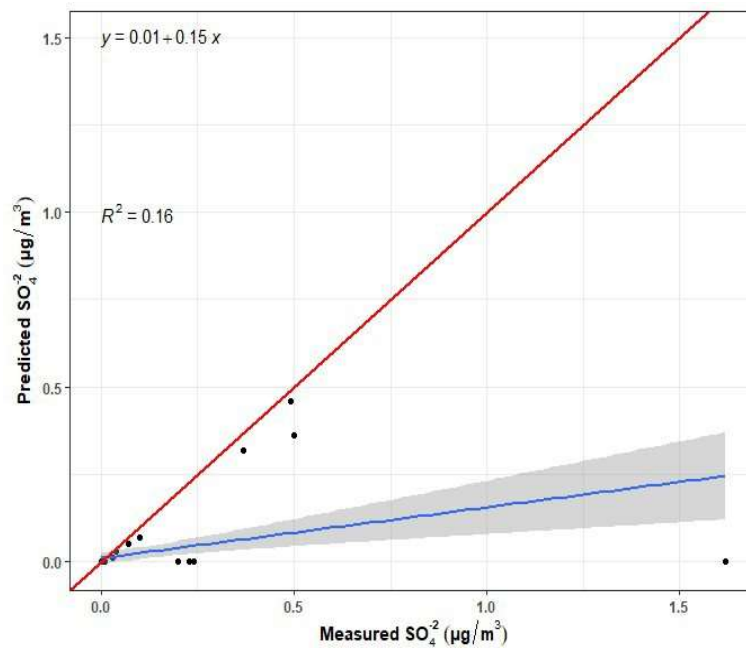


Figure 3.13. ISORROPIA-II predicted  $\text{SO}_4^{2-}$  vs. measured  $\text{SO}_4^{2-}$  under stable state conditions with 1:1 slope line (red), regression line (blue), and 95% confidence interval (gray area)

### 3.4.3 Response of Secondary $iPM_{2.5}$ to Total $NH_3$

Inputs for the sensitivity analysis are summarized in Table 3.5. Average total  $SO_4^{-2}$  and average total  $NO_3^-$  of measured data were used under five different temperatures and RH combinations of measured data to analyze the secondary formation of  $iPM_{2.5}$  with increasing total  $NH_3$ .

**Table 3.5. ISORROPPIA-II sensitivity analysis inputs**

Input Variables	Minimum	Median	Maximum	Mean
Total $SO_4^{-2}$	0	0	1.62	0.053
Total $NH_3$	0.18	0.78	4.28	1.06
Total $NO_3^-$	0	0.07	2.88	0.30
RH (%)	68	78	88	77
T (K)	274.07	295.09	300.26	288.95

The response of  $iPM_{2.5}$  to total  $NH_3$  is shown in Figure 3.14. Under maximum temperature + minimum RH (300 K + 68%), there was no response from  $iPM_{2.5}$  to increasing total  $NH_3$ . At maximum temperature + maximum RH (300 K + 88%), there was once again no response from  $iPM_{2.5}$ . At medium temperature + median RH (295 K + 78%),  $iPM_{2.5}$  was insensitive to increasing total  $NH_3$ . The lack of response from  $iPM_{2.5}$  to increasing total  $NH_3$  in this temperature range can be attributed to the fact that the high temperature and RH measured at this site did not favor the formation of  $NH_4NO_3$  even with  $NH_3$  rich conditions which agrees with the observation made by Cheng et al., (2021) and Dawson et al., (2007). Since  $SO_4^{-2}$  concentrations were at or near 0, there was no  $SO_4^{-2}$  dominant  $iPM_{2.5}$  formed in the warmer temperatures. Under minimum temperature + maximum RH (274 K + 88%), increasing total  $NH_3$  increases  $iPM_{2.5}$ . At minimum temperature + minimum RH (274 K + 68%),  $iPM_{2.5}$  also increased with increasing total  $NH_3$ , which relates to lower temperatures favoring  $NH_4NO_3$  formation. There was a larger

response of  $iPM_{2.5}$  when RH was higher, which indicates that higher RH was favorable for  $NH_4NO_3$  formation at low temperatures. The increase in  $NO_3^-$ ,  $NH_4^+$ , and  $iPM_{2.5}$  in both cases was halted when  $HNO_3$  approached 0.

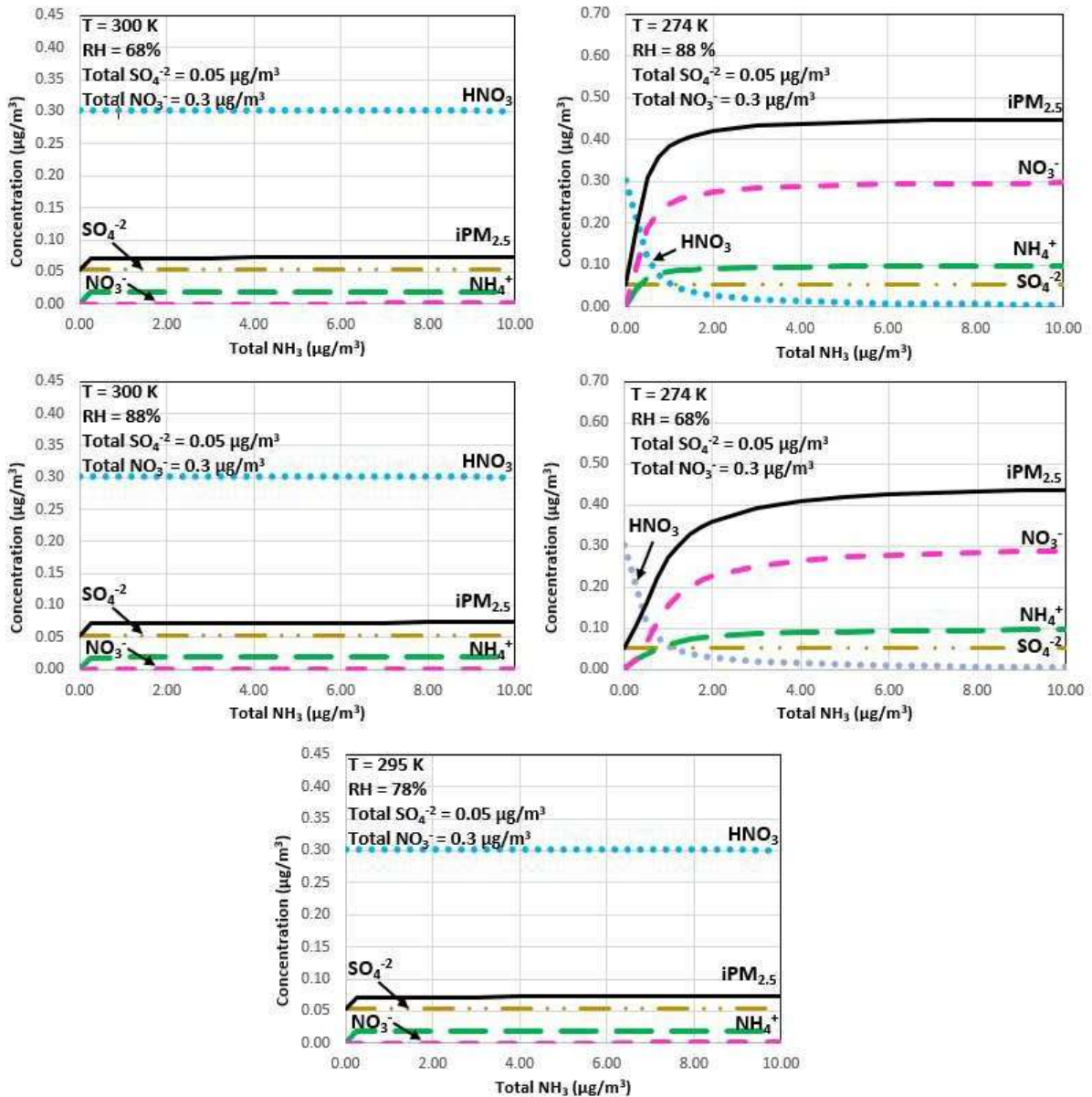


Figure 3.14. Responses of  $iPM_{2.5}$  components to total  $NH_3$  under five different T and RH conditions

#### **3.4.4 Response of Secondary $iPM_{2.5}$ to Total $NO_3^-$**

Average total  $SO_4^{2-}$  and average total  $NH_3$  were simulated under five different temperatures and RH combination to analyze the secondary formation of  $iPM_{2.5}$  with increasing total  $NO_3^-$ . The response of  $iPM_{2.5}$  to total  $NO_3^-$  is shown in Figure 3.15. Under maximum temperature + minimum RH (300 K + 68%), maximum temperature + maximum RH (300 K + 88%), and median temperature + median RH (295 K + 78%), there was no response from  $iPM_{2.5}$  with increasing total  $NO_3^-$ . This is once again due to the fact that higher temperatures did not favor  $NH_4NO_3$  formation despite the concentration of  $NO_3^-$  being higher than  $SO_4^{2-}$ . Under minimum temperature + maximum RH (274 K + 88%), and minimum temperature + minimum RH (274 K + 68%), there was a response of  $iPM_{2.5}$  with increasing total  $NO_3^-$ . Similar to Figure 3.12,  $iPM_{2.5}$  increased until all  $NH_3$  reacted with  $HNO_3$ . At the maximum RH, there was a higher concentration of  $iPM_{2.5}$  compared to the concentration at the minimum RH. This suggests that  $NH_4NO_3$  formation favors higher RH when temperature is at or below 274 K.

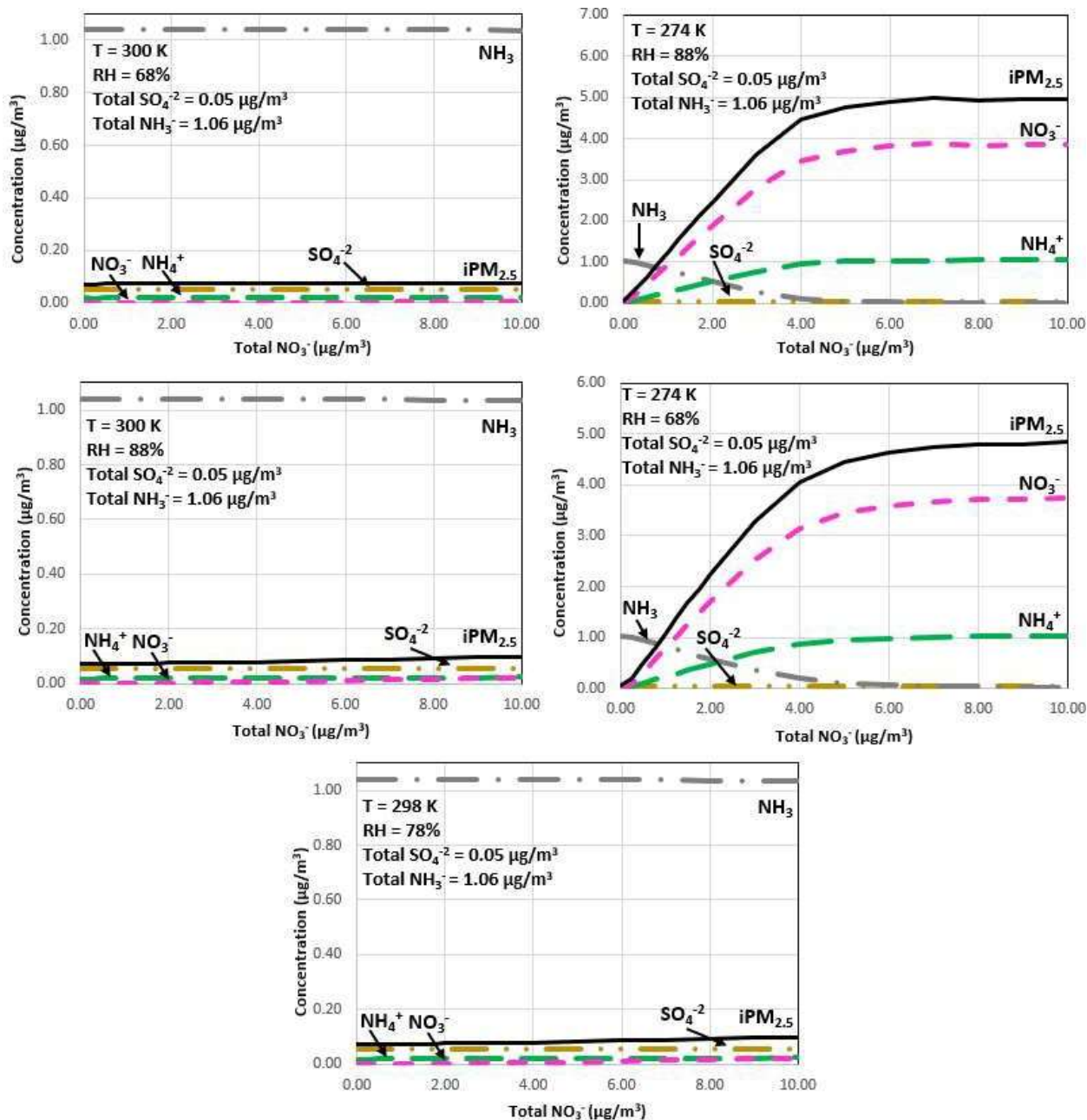


Figure 3.15. Responses of  $\text{iPM}_{2.5}$  components to total  $\text{NO}_3^-$  under five different T and RH conditions

For both cases of the sensitivity analysis, there was no response of  $\text{iPM}_{2.5}$  with increasing total  $\text{NH}_3$  and total  $\text{NO}_3^-$  when temperature was high. Previous research from Dawson et al., (2007), Cheng et al., (2019a), and Li et al., (2014a) observed that  $\text{iPM}_{2.5}$  concentrations were higher in the summer than the winter since  $(\text{NH}_4)_2\text{SO}_4$  formation was favored at high temperatures; however, the low availability of ambient  $\text{SO}_2$  limited  $(\text{NH}_4)_2\text{SO}_4$  formation at this

research site. Even though there was more available  $\text{HNO}_3$  than  $\text{H}_2\text{SO}_4$  in the summer, no reaction occurred with  $\text{NH}_3$ . Previous research from Cheng et al. (2021) and Pacyna et al., (1996) found that  $\text{HNO}_3$  is more volatile than  $\text{H}_2\text{SO}_4$  and higher temperatures may decompose  $\text{NH}_4\text{NO}_3$  into gas-phase  $\text{NH}_3$  and  $\text{HNO}_3$  allowing  $\text{SO}_4^{2-}$  to be the dominant anion in the formation of  $\text{iPM}_{2.5}$  during the summer. For this research, since the median temperature was only 2 K less than the maximum, there was no response from  $\text{iPM}_{2.5}$  with increasing total  $\text{NH}_3$  and total  $\text{NO}_3^-$ . For simulations where temperature was low, there was a response of  $\text{iPM}_{2.5}$  for both cases with increasing total  $\text{NH}_3$  and total  $\text{HNO}_3$ . For increasing  $\text{NH}_3$ ,  $\text{iPM}_{2.5}$  increased to approximately  $0.45 \mu\text{g}/\text{m}^3$  while increasing total  $\text{NO}_3^-$  increased  $\text{iPM}_{2.5}$  to approximately  $5 \mu\text{g}/\text{m}^3$ . The greater response from increasing total  $\text{NO}_3^-$  is an indication that secondary  $\text{iPM}_{2.5}$  formation was limited to the availability of  $\text{HNO}_3$ . The response of  $\text{iPM}_{2.5}$  for both cases of the sensitivity analysis indicate that secondary  $\text{iPM}_{2.5}$  formation was more sensitive to  $\text{H}_2\text{SO}_4$  and  $\text{HNO}_3$  than  $\text{NH}_3$ . These observations agree with the findings presented by Cheng et al., (2019b) and Walker (2006) where a sensitivity analysis was conducted at two different sites in NC where  $\text{iPM}_{2.5}$  precursor gases were abundant.

## CHAPTER 4: CONCLUSIONS AND FUTURE WORK

The major finding of this research on the PM<sub>2.5</sub> chemical speciation, atmospheric chemical conditions, and iPM<sub>2.5</sub> formation as impacted by atmospheric chemical and meteorological conditions in a poultry production environment include the following:

- 1) The PM<sub>2.5</sub> at the research site was dominant in OC ranging between 80% to 94% of total composition.
- 2) The NH<sub>3</sub>-related iPM<sub>2.5</sub> was insignificant in PM<sub>2.5</sub> composition ranging between 0% to 2%. The dominant anion in iPM<sub>2.5</sub> composition was NO<sub>3</sub><sup>-</sup>.
- 3) In this rural environment, more available HNO<sub>3</sub> promoted iPM<sub>2.5</sub> formation when T ≤ 274 K.
- 4) The ISORROPIA-II model predicted NO<sub>3</sub><sup>-</sup>, SO<sub>4</sub><sup>-2</sup>, and NH<sub>3</sub> well, but poorly predicted NH<sub>4</sub><sup>+</sup> where OC was the dominant fraction in PM<sub>2.5</sub> composition.
- 5) Ambient NH<sub>3</sub> near the AFO was sufficient; however, insufficient H<sub>2</sub>SO<sub>4</sub> and HNO<sub>3</sub> limited NH<sub>3</sub> neutralization potential, which further limited the secondary formation of iPM<sub>2.5</sub>.

Through the fieldwork and data analysis, the following suggestions are provided to enhance the research findings of future work:

- Collect 24-hour ambient precursor gas concentrations data to replace passive sampling assessment
- Collect 3 years of data for all seasons with sufficient replicates
- Further assessment of the spatial and temporal variations of atmospheric chemical parameters in all wind directions

- ISORROPIA-II modeling and comparing the stable and metastable state under different temperatures and RH
- Further investigate the effects of OC/PM<sub>2.5</sub> on iPM<sub>2.5</sub> formation

## REFERENCES

- Almaraz, M., Bai, E., Wang, C., Trousdell, J., Conley, S., Faloona, I., & Houlton, B. Z. (2017). Agriculture is a major source of NO<sub>x</sub> pollution in California. *Science Advances*, 4. <https://doi.org/aa03477>
- Anlauf, K.G., Fellin, P., Wiebe, H.A., Schiff, H.I., Mackay, G.I., Braman, R.S., & Gilbert, R. (1985). A comparison of three methods for measurement of atmospheric nitric acid and aerosol nitrate and ammonium. *Atmos Environ*, 19 (2), 325–333.
- Anttila, T., Kiendler-Scharr, A., Mentel, T. F., and Tillmann, R. (2007) Size dependent partitioning of organic material: evidence for the formation of organic coatings on aqueous aerosols. *J. Atmos. Chem.*, 57, 215–237, doi:10.1007/s10874-007-9067-9.
- Asman, W., & Jensen A. (1993). A long-range transport model for ammonia and ammonium for Europe. *Atmospheric Environment*, 21, 2099-2119.
- Asman, W. (1994). Emission and deposition of ammonia and ammonium. *Nova Acta Leopoldina NF*, 70, 263-297.
- Asman, W., Sutton, M., & Schjørring, J. (1998). Ammonia: emission, atmospheric transport and deposition. *New Phytologist*, 139, 27-48.
- Bauer, S., Tsigaridis, K., & Miller, R. (2016). Significant atmospheric aerosol pollution caused by world food cultivation. *Geophys. Res. Lett*, 43, 5394-5400.
- Behera, S., Sharma, M., Aneja, V., & Balasubramanian, R. (2013). Ammonia in the atmosphere: a review on emissions sources, atmospheric chemistry and deposition on terrestrial bodies. *Environmental Science and Pollution Research*, 20, 8092-8131.
- Bertram, A. K., Martin, S. T., Hanna, S. J., Smith, M. L., Bodsworth, A., Chen, Q., Kuwata, M., Liu, A., You, Y., and Zorn, S. R. (2011). Predicting the relative humidities of liquid-liquid phase separation, efflorescence, and deliquescence of mixed particles of

- ammonium sulfate, organic material, and water using the organic-to-sulfate mass ratio of the particle and the oxygen-to carbon elemental ratio of the organic component. *Atmos. Chem. Phys.*, *11*, 10995–11006, doi:10.5194/acp-11-10995-2011.
- Blanes-Vidal, V., Nadimi, E., Ellermann, T., Andersen, H., & Løfstrøm, P. (2012). Perceived annoyance from environmental odors and association with atmospheric ammonia levels in non-urban residential communities: a cross-sectional study. *Environ. Health: Global Access Sci.*, *11*, 1-10.
- Bobbink, R., Hornung, M., & Roelofs, J. (1998). The effects of air-borne nitrogen pollutants on species diversity in natural and semi-natural European vegetation. *J. Ecol.*, *86*, 717-738.
- Bobbink, R., & Hicks, K. (2014). Factors affecting N deposition impacts on biodiversity: an overview. *Nitrogen Deposition, Critical Loads and Biodiversity*, 127-138.
- Bouwman, A.F., Van Vuuren, D.P., Derwent, R.G., & Posch, M. (2002). A global analysis of acidification and eutrophication of terrestrial ecosystems. *Water, Air, and Soil Pollution*, *141*, 349-382
- Bu, X., Xie, Z., Liu, J., Wei, L., Wang, X., Chen, M., & Ren, H. (2017). Global PM<sub>2.5</sub>-attributable health burden from 1990 to 2017: Estimates from the Global Burden of disease study 2017. *Environmental Research*, *197*.
- CAFRE (College of Agriculture, Food, & Rural Enterprise), (2020). Low Emission Slurry Spreading Systems help to reduce ammonia emissions. Available at <https://niopa.qub.ac.uk/bitstream/NIOPA/11217/1/low-emission-slurry-spreading-systems-help-to-reduce-ammonia-emissions-Jan-2020.pdf>

- CFR. *Reference method for the determination of fine particulate matter as PM<sub>2.5</sub> in the atmosphere*, 40 CFR, Part 50, Appendix L; U.S. Government Printing Office: Washington, DC
- Chen, Z., Liu, J., Liu, M., You, R., & He, S. (2021). An Aerosol Sensor for Multi-Sized Particles Detection Based on Surface Acoustic Wave Resonator and Cascade Impactor. *Applied Sciences*, *11*, 9833
- Cheng, B., Wang-Li, L., Meskhidze, N., Classen, J., & Bloomfield, P. (2022), Performance of a Thermodynamic Model for Predicting Inorganic Aerosols in the Southeastern U.S. *Atmosphere*, *13*.
- Cheng, B., Wang-Li, L., Meskhidze, N., Classen, J., & Bloomfield, P. (2021). Partitioning of NH<sub>3</sub>-NH<sub>4</sub><sup>+</sup> in the Southeastern U.S. *Atmosphere*, *12*, 1681.
- Cheng, B., Wang-Li, L., Meskhidze, N., Classen, J., & Bloomfield, P. (2019a) Spatial and temporal variations of PM<sub>2.5</sub> mass closure and inorganic PM<sub>2.5</sub> in the Southeastern U.S. *Environmental Science and Pollution Research*, *26*, 33181-33191
- Cheng, B., Wang-Li, L., (2019b) Responses of Secondary Inorganic PM<sub>2.5</sub> to Precursor Gases in an Ammonia Abundant Area in North Carolina. *Aerosol and Air Quality Research*, *19*, 1126-1138.
- Ciobanu, V. G., Marcolli, C., Krieger, U. K., Weers, U., and Peter, T. (2009) Liquid-Liquid Phase Separation in Mixed Organic/Inorganic Aerosol Particles. *J. Phys. Chem. A*, *113*, 10966–10978, doi:10.1021/jp905054d.
- Dawson, J.P., Adams, P.J., & Pandis, S.N. (2007). Sensitivity of PM<sub>2.5</sub> to climate in the Eastern US: a modeling case study. *Atmospheric Chemistry and Physics*, *7*, 4295–4309.

- Dietrich, Y.Z. (2019). Improvement and Application of a New Ammonia Emission Inventory for Poultry and Swine Production in North Carolina. PhD. Dissertation. Department of Biological and Agricultural Engineering, North Carolina State University
- Elliot, H. A., & Collins N. E. (1982) Factors affecting ammonia release in broiler houses. *Trans. ASAE*, 25, 413–418.
- EPA (2020). Quality Assurance Project Plan. Available at [https://www.epa.gov/sites/default/files/2020-07/documents/csn\\_shipping\\_and\\_handling\\_qapp.pdf](https://www.epa.gov/sites/default/files/2020-07/documents/csn_shipping_and_handling_qapp.pdf).
- EPA (2017) Ambient atmospheric ammonia in Ireland. Available at [https://www.epa.ie/publications/research/air/EPA-RR-193-Essentra-web-\(1\).pdf](https://www.epa.ie/publications/research/air/EPA-RR-193-Essentra-web-(1).pdf)
- EPA (1999). Nitrogen Oxides (NO<sub>x</sub>) Why and How They Are Controlled. Available at <https://www3.epa.gov/ttnca1/dir1/fnoxdoc.pdf>
- EPA (Environmental Protection Agency), (1979) Current Methods to Measure Atmospheric Nitric Acid and Nitrate Artifacts. Available at <https://nepis.epa.gov/Exe/ZyPDF.cgi/910185Q4.PDF?Dockey=910185Q4.PDF>
- Fountoukis, C., & Nenes, A. (2007) ISORROPIA II: A computationally efficient thermodynamic equilibrium model for K<sup>+</sup>-Ca<sup>2+</sup>-Mg<sup>2+</sup>-NH<sub>4</sub><sup>+</sup>-Na<sup>+</sup>-SO<sub>4</sub><sup>2-</sup>-NO<sub>3</sub><sup>-</sup>-Cl<sup>-</sup>-H<sub>2</sub>O aerosols. *Atmospheric Chemistry and Physics*, 7, 4639-4659.
- Grantz, D.A., Garner, J.H.B., & Johnson, D.W. (2003). Ecological Effects of Particulate Matter. *Environmental International*, 29, 213-239.
- Guo, H., Nenes, A., & Weber R.J. (2018). The underappreciated role of nonvolatile cations on aerosol ammonium-sulfate molar ratios. *Atmos. Chem. Phys.*, 18, 17307–17323

- Guthrie, S., Giles, S., Dunkerley, F., Tabaqchali, H., Harshfield, A., Ioppolo, B., & Manville, C. (2018). Impact of ammonia emissions from agriculture on biodiversity. *RAND Corporation*, 76.
- Harrison, R., Jones, A., & Lawrence, R. (2004). Major Component composition of PM<sub>10</sub> and PM<sub>2.5</sub> from roadside and urban background sites. *Atmospheric Environment*, 38, 4351-4538.
- Jiang J., Stevenson, D., Uwizeye, A., Tempio, G., & Sutton M. (2021). A climate-dependent global model of ammonia emissions from chicken farming. *Biogeosciences*, 18, 135-158.
- Koop, T., Bookhold, J., Shiraiwa, M., and Pöschl, U. (2011). Glass transition and phase state of organic compounds: dependency on molecular properties and implications for secondary organic aerosols in the atmosphere. *Phys. Chem. Chem. Phys.*, 13, 19238–19255, doi:10.1039/c1cp22617g.
- Koziel, J.A., Aneja, V.P., & Baek B.H. (2006). Gas-to-particle conversion process between ammonia, acid gases, and fine particles in the atmosphere. *Agricultural and Biosystems Engineering Publications.*, 67, 201-224. [https://lib.dr.iastate.edu/abe\\_eng\\_pubs/67](https://lib.dr.iastate.edu/abe_eng_pubs/67)
- Kupper, T., Hani, C., Neftel, A., Kincaid, C., Buhler, M., Amon, B., VanderZaag, A. (2020). Ammonia and greenhouse gas emissions from slurry storage- a review. *Agriculture, Ecosystems, and Environment*, 300.
- Lee, C., Randall, M., Donkelaar, A., Lee, H., Dickerson, R., Hains, J., Krotkov, N., Richter, A., Vinnikov, K., & Schwab, J. (2011). SO<sub>2</sub> emissions and lifetimes: Estimates from inverse modeling using in situ and global, space-based (SCIAMACHY and OMI) observations. *J.G.R.*, 116.

- Lelieveld, J., Evans, J.S., Fnais, M., Giannadaki, D., & Pozzer, A. (2015). The contribution of outdoor air pollution sources to premature mortality on a global scale. *Nature*, *525*, 367-371.
- Li, Q-F., Wang-Li, L., Liu, Z., Jayanty, R.K.M., Shah, S.B., & Bloomfield, P. (2014a). Ammonia concentrations and modeling of inorganic particulate matter in the vicinity of an egg production facility in Southeastern USA. *Environ. Sci. Pollut. Res.*, *21*, 4675-4685.
- Li, Q-F., Wang-Li, L., Liu, Z., Jayanty, R.K.M., Shah, S.B., & Bloomfield, P. (2014b). Major Ionic Composition of Fine Particulate Matter in an Animal Feeding Operation Facility and its Vicinity. *J. Air Waste Manage. Assoc.*, *21*, 1279-1287.
- Liggio, J., Li, S.M., Vlasenko, A., Stroud, C., & P. Makar (2011). Depression of ammonia uptake to sulfuric acid aerosols by competing uptake of ambient organic gases. *Environ. Sci. Technol.*, *45*, 2790–2796.
- Liu, F., Beirle, S., Zhang, Q., Dörner, S., He, K. & Wagner, T. (2016). NO<sub>x</sub> lifetimes and emissions of cities and power plants in polluted background estimated by satellite observations *Atmos. Chem. Phys.*, *16*, 5283-5298.
- Ma, R., Zou, J., Han, Z., Yu, K., Wu, S., Liu, S., Niu, S., Horwath W., & Zhu-Barker, X. (2020). Global soil-derived ammonia emissions from agricultural nitrogen fertilizer application: A refinement based on regional and crop-specific emission factors. *Global Change Biology*, *27*, 855-867.
- Makar, P. A., Moran, M. D., Zheng, Q., Cousineau, S., Sassi, M., Duhamel, A., Besner, M., Davignon, D., Crevier, L. P., & Bouchet, V. S. (2009). Modelling the impacts of

- ammonia emissions reductions on North American air quality. *Atmos. Chem. Phys. Discuss.*, 2, 5371-5422.
- Malley, C., Hicks, W., Kulyenstierna, C., Michalopoulou, E., Molotoks, A., Slater, J., Heaps, C., Ulloa, S., Veysey J., & Shindell, D. (2021). Integrated assessment of global climate, air pollution, and dietary, malnutrition and obesity health impacts of food production and consumption between 2014 and 2018. *Environ. Res. Commun.*, 3.
- Masia P., Dipalo V., & Possanzini M (1994) Uptake of ammonia by nylon filters in filter pack systems. *Atmos Environ.*, 2, 365–366
- Mehlmann A., Warneck P. (1995) Atmospheric gaseous HNO<sub>3</sub> particulate nitrate, and aerosol-size distributions of major ionic species at a rural site in western Germany. *Atmos. Environ.*, 17, 2359–2373
- Mendes, L., Pieters, J., Snoek, D., Ogink, N., Brusselman, E., & Demeyer, P. (2017). Reduction of ammonia emissions from dairy cattle cubicle houses via improved management- or design-based strategies: A modeling approach. *Science of the Total Environment*, 574, 520-531.
- Meng, Z., & Seinfeld, J. (1996). Atmospheric gas-aerosol equilibrium IV. Thermodynamics of carbonations. *Aerosol Science Technology*, 23, 131-154.
- Moya, M., Pandis, S.N., & Jacobson, M.Z. (2002). Is the size distribution of urban aerosols determined by thermodynamic equilibrium? An application to Southern California. *Atmos. Environ.*, 36, 2349–2365.
- Na, K., Sawant, A., Song, C., & Cocker III, D. (2004). Primary and secondary carbonaceous species in the atmospheric of Western Riverside County, California. *Atmospheric Environment*, 38, 1345-1355.

- Novriyanti, E., Watanbe, M., Koike, T. (2022). The Atmospheric Concentration of Common Greenhouse Gases in the Pulpwood Plantation in Riau Province, Indonesia. IOP Conference Series: Earth and Environmental Science.
- Ogawausa (2006). NO, NO<sub>2</sub>, NO<sub>x</sub>, and SO<sub>2</sub> Sampling Protocol Using The Ogawa Sampler [http://ogawausa.com/wp-content/uploads/2017/11/prono-noxno2so206\\_206\\_1117.pdf](http://ogawausa.com/wp-content/uploads/2017/11/prono-noxno2so206_206_1117.pdf)
- Pacyna, J. M., & Benson, S. (1996). Gas-to-particle conversion of sulfur and nitrogen compounds as studied at marine stations in Northern Europe. *Atmospheric Environment*, 18, 3129-3140.
- Phillips, S., Arya, S., & Aneja, V. (2004). Ammonia flux and dry deposition velocity from near-surface concentration gradient measurements over a grass surface in North Carolina. *Atmospheric Environment*, 38, 3469-3480.
- Ravishankara, A.R., (1997). Heterogeneous and multiphase chemistry in the troposphere. *Science*, 276, 1058–1065.
- Saarikoski, S., Timonen, H., Saarnio, K., Aurela, M., Jarvi, L., Keronen, P., Kerminen, V.-M., & Hillamo, R. (2008). Sources of organic carbon in fine particulate matter in northern European urban air. *Atmospheric, Chemistry, and Physics*, 8, 6281-6295.
- Seinfeld, J.H., & Pandis, S.N., (1998). *Atmospheric Chemistry and Physics, from Air Pollution to Climate Change*.
- Sharon, H., Matson, P., & Roth, P. (1996). NO<sub>x</sub> EMISSIONS FROM SOIL: Implications for Air Quality Modeling in Agricultural Regions. *Annual Review of Energy and the Environment*, 21, 311-346

- Shaver, S., Leytem, A., Burns, R., Xin, H., Wang-Li, L., Moody, L., Embertson, N., & Fabian-Wheeler, E. (2014). Ammonia Emissions: What to Know Before You Regulate. Prepared by the United States Department of Agriculture, Agricultural Air Quality Task Force.
- Silvern, R., Jacob, D., Kim, P., Marais, E., Turner, J., Campuzano-Jost, P., & Jimenez, J. (2017). Inconsistency of ammonium–sulfate aerosol ratios with thermodynamic models in the eastern US: a possible role of organic aerosol. *Atmos. Chem. Phys.*, *17*, 5107-5118, <https://doi.org/10.5194/acp-17-5107-2017>, 2017.
- Sommer, S.G., Olesen, J.E., & Christensen, B.T. (1991). Effects of temperature, wind speed and air humidity on ammonia volatilization from surface applied cattle slurry. *J. Agric. Sci.*, *117*, 91-100.
- Sturges W.T., & Harrison R.M. (1989). The use of nylon filters to collect Hcl:efficiencies, interferences and ambient concentrations. *Atmos Environ*, *9*, 1987–1996
- Sutton, M.A., Fowler, D., & Moncrieff, J.B. (1993). The exchange of atmospheric ammonia with vegetated surfaces. I. Unfertilized vegetation. *Quarterly Journal of the Royal Meteorology Society*, *119*, 1023-1045.
- Sutton, M.A., Schjørring, J.K., & Wyers, G.P. (1995). Plant atmosphere exchange of ammonia. *Philosophical Transactions of the Royal Society*, *351*, 261-278.
- Sutton, M.A., Reis, S., Riddick, S., Dragosits, U., Nemitz, E., Theobald, M., Tang, Y., Braban, C., Vieno, M., Dore, A., Mitchell, R., Wanless, S., Daunt, F., Fowler, D., Blackall, T., Milford, C., Flechard, C., Loubet, B., Massad, R., Cellier, P., Personne, E., Coheur, P., Clarisse, L., Van Dammne, M., Ngadi, Y., Clerbaux, C., Skøth, C., Geels, C., Hertel, O., Kruit, R., Pinder, R., Bash, J., Walker, J., Simpson, D., Horvath, L., Misselbrook, T.,

- Bleeker, A., Dentener, F., & de Vries, W., (2013). Towards a climate-dependent paradigm of ammonia emission and deposition. *Phil Trans R Soc B*, 368.
- Van Damme, M., Clarisse, L., Franco, B., Sutton, M., Erisman, J., Kruit, R., Zanten, M., Whitburn, S., Hadji-Lazarou, J., Hurtmans, D., Clerbaux, C., & Coheur, P. (2021). Global, regional and national trends of atmospheric ammonia derived from a decadal (2008–2018) satellite record. *Environmental Research Letters*, 16.
- Van Hove, L.W.A., Adema, E.H., Vredenburg, W.J., & Pieters, G.A. (1989). A study of the adsorption of NH<sub>3</sub> and SO<sub>2</sub> on leaf surfaces. *Atmospheric Environment*, 23, 1479-1486.
- Walker, J.T., Robarge, W.P., Shendrikar A., & Kimball, H. (2006). Inorganic PM<sub>2.5</sub> at a US agricultural site. *Environ. Pollut.*, 2, 258–271
- Walker, J.T., Aneja, V.P., & Dickey, D.A. (2000). Atmospheric transport and wet deposition of ammonium in North Carolina. *Atmospheric Environment* 34, 3407-3418
- Wang, G., Cheng, S., Li, J., Lang, J., Wen, W., Yang, X., & Tian, L. (2015). Source apportionment and seasonal variation of PM<sub>2.5</sub> carbonaceous aerosol in the Beijing-Tianjin-Hebei Region of China. *Environmental Monitoring and Assessment*, 187.
- Wang-Li, L. 2013. Techniques for characterization of particulate matter emitted from animal feeding operations. *American Chemical Society (ACS)*, 15-39. DOI: 10.1021/bk-2013-1126.ch002.
- Webb, J., Menzi, H., Pain, B.F., Misselbrook, T.H., Dammgren, U., Hendriks, H., & Dohler, H. (2005). Managing ammonia emissions from livestock production in Europe. *Environmental Pollution*, 135, 399-406.
- Wexler, A.S., & Seinfeld, J.H. (1992). Analysis of aerosol ammonium nitrate: Departures from equilibrium during SCAQS. *Atmos. Environ.*, 26, 579–591

Wing, S., & Susanne, W. (2000). Intensive Livestock Operations, Health, and Quality of Life among Eastern North Carolina Residents. *Environmental Health Perspectives*, 108.

World Health Organization (2013). Health effects of Particulate Matter.

Wu, S-Y., J-L. Hu, Y. Zhang, & Aneja V.P. (2007). Modeling atmospheric transport and fate of ammonia in North Carolina-Part II: effect of ammonia emissions on fine particulate matter formation. *Atmos. Environ.* 42, 3437-3451.

Xu, J., Chen, J., Wang, G., Yu, G., Li, H., Huo, J., Lin, Y., Fu, Q., Guo, H., Deng, C., Lee, S-H, Chen, J., & Huang, K. Importance of gas-particle partitioning of ammonia in haze formation in the rural agricultural environment. *Atmos. Chem. Phys.*, 20, 7259-7269

You, Y., Renbaum-Wolff, L., and Bertram, A. K. (2013) Liquid-liquid phase separation in particles containing organics mixed with ammonium sulfate, ammonium bisulfate, ammonium nitrate or sodium chloride. *Atmos. Chem. Phys.*, 13, 11723–11734, doi:10.5194/acp-13-11723-2013.